Accepted Manuscript

Geological Society, London, Special Publications

Structure and kinematics of the Central Sivas Basin (Turkey): Salt deposition and tectonics in an evolving fold-and-thrust belt

Etienne Legeay, Jean-Claude Ringenbach, Charlie Kergaravat, Alexandre Pichat, Geoffroy Mohn, Jaume Vergés, Kaan Sevki Kavak & Jean-Paul Callot

DOI: https://doi.org/10.1144/SP490-2019-92

Received 13 May 2018
Revised 23 March 2019
Accepted 23 April 2019

Structure and kinematics of the Central Sivas Basin (Turkey): Salt deposition and tectonics in an evolving fold-and-thrust belt

Etienne LEGEAY [1, 2]*, Jean-Claude RINGENBACH [2], Charlie KERGARAVAT [2], Alexandre PICHAT [1, 2], Geoffroy MOHN [3], Jaume VERGÉS [4], Kaan Sevki KAVAK [5], Jean-Paul CALLOT [1]

E2S UPPA CNRS /TOTAL/Univ Pau & Pays Adour, Laboratoire Des Fluides Complexes Et Leurs Reservoirs-IPRA, UMR5150, Pau, France.

[2] Total SA, CSTJF, Pau, France

[3] Géosciences Environnement Cergy, Université de Cergy-Pontoise, Cergy-Pontoise, France

[4] Group of Dynamics of the Lithosphere, Institute of Earth Sciences Jaume Almera, ICTJA-CSIC, Barcelona, Spain

[5] Department of Geological Engineering, Sivas Cumhuriyet University, Sivas, Turkey

*Corresponding author: etienne.legeay@gmail.com

Key Points

- 2D seismic and fieldwork data coverage in the Sivas Basin.
- Evolution of multi-décollement fold-and-thrust belt.
- Development of a synorogenic halokinetic foreland.

Keywords

Sivas Basin

Anatolia

Fold-and-Thrust Belt

Salt and Thrust Belt

Salt Tectonics

Synorogenic salt

ABSTRACT

The Sivas Basin in central-eastern Anatolia is a north-verging salt-bearing fold-and-thrust belt including synorogenic salt tectonics. It formed between the northern leading edge of the Taurides platform and the Kırşehir block since Late Cretaceous time.

We have constructed five regional cross-sections supported by field data and 2D seismic to constrain the structure of the basin and its evolution. The area is divided into three tectonic domains from south to north: (i) a Maastrichtian to Eocene north-verging fold-and-thrust belt, which terminates by a regional Eocene evaporitic level, (ii) an Oligo-Miocene salt domain which contains two generations of minibasins separated by a salt canopy, forming a salt-and-thrust belt, and (iii) a Late Miocene to present day foreland basin.

The cross-sections show the along-strike variations and the increasing shortening in the fold-and-thrust belt from west (~15 km) to east (~25 km). The thick salt allows for the intracutaneous propagation of the fold-and-thrust belt below a domain of salt withdrawal minibasins, decoupled as the initial salt thickness increases. In that case, the salt domain is thrusted both frontward and backward. Efficient exhumation then erosion of the fold-and-thrust resulting in synorogenic salt tectonics in the foreland and thus increasing the mechanical resistance between them.

INTRODUCTION

Fold-and-thrust belts (FTBs) and related foreland basins in the world accommodate crustal convergence (Hardy et al. 1998; Ford 2004; Pfiffner 2006; Mouthereau et al. 2013). The structure of FTBs is analysed in terms of both thin- and thick-skinned tectonics in the hinterland and mostly thin-skinned in the outer domain toward the foreland (Pfiffner 2006; Mouthereau et al. 2013; Lacombe & Bellahsen 2016). Shortening in a FTB is accommodated through in-sequence or/and out-of-sequence thrusting and associated folding in order to preserve the critical taper angle of the orogenic wedge, which is modulated by erosion and sedimentation (Davis et al. 1983; Dahlen et al. 1984; Davis & Engelder 1985; Beaumont et al. 1992; Mugnier et al. 1997; Couzens-Schultz et al. 2003; Graveleau & Dominguez 2008; Fillon et al. 2013). The presence of intra-wedge décollement levels promotes the formation of

a large set of contractional structures, such as ramp-flat, imbricate thrusts or duplex (Boyer & Elliot 1982). The internal stacking of thrust slices between a basal décollement and an upper décollement (i.e. a roof thrust) forms triangle zones geometries which are quite common at the front of FTBs (MacKay et al. 1996). The kinematic of a roof thrusting with forward propagation (i.e. toward the foreland) is called "active-roof thrust", in contrast to a backward propagation (i.e. toward the hinterland) called "passive-roof thrust" (see review in von Hagke & Malz 2018). Such geometries are controlled by the spatial distribution of the décollements (their overlaps and relative vertical position), their thickness variations and their rheologies, as observed in natural examples and analogue models (e.g. Couzens-Schultz et al. 2003; Feng et al. 2015; Santolaria et al. 2015; von Hagke & Malz 2018 and references therein).

The rheology of a décollement level can be viscous (e.g. evaporites) or frictional (e.g. shales) (Weijermars & Schmeling 1986; Costa & Vendeville 2002; Couzens-Schultz et al. 2003; Duffy et al. 2018). In the case of a viscous décollement, the taper dynamic and the shape of a FTB differ largely from the classic frictional case: (1) the propagation of the deformation front is faster and reaches first the pinch-out of the décollement level; (2) the deformation sequence is dependent of the evaporite thickness distribution and heterogeneities within the sedimentary pile (e.g. diapirs); and (3) the wedge taper is low (Davis & Engelder 1985; Letouzey et al. 1995; Talbot & Alavi 1996; Cotton & Koyi 2000; Costa & Vendeville 2002; Ford 2004; Duffy et al. 2018).

Salt-influenced FTBs can be described through three main structural styles (see review in Duffy et al. 2018). In classical salt-detached FTBs, the salt acts as an efficient décollement layer without precursor salt structures, such as in the Jura Mountains (e.g. Laubscher 1972; Davis & Engelder 1985), the Northwestern Zagros (e.g. Talbot & Alavi 1996; Sherkati et al. 2006) or in the Salt range in Pakistan (e.g. Butler et al. 1987; Cotton & Koyi 2000; Ghani et al. 2018). Alternatively, pre-shortening salt structures (i.e. diapirs and salt walls) are present and act as weakness zones that contribute to strain localization, folding, thrusting or salt extrusion, such as in the Fars Province in Zagros Mountains (Callot et al. 2012; Callot et al. 2007; Jahani et al. 2009) or in the Paradox Basin in Utah (Raup & Hite 1992; Barbeau 2003). The third style of salt-influenced FTB involves those marked by a very important initial salt stock having favoured the formation of minibasins and canopies prior to and during shortening, such as in the Guadalquivir Basin (Berástegui et al. 1998; Flinch & Soto 2017), the Axel Heiberg Basin (Jackson & Harrison 2006; Harrison & Jackson 2014) or in the Sivas Basin (Legeay et al., 2018; Kergaravat et al. 2018). Salt-related FTBs can be

compared with offshore gravitational FTBs, in which shortening related to gravity gliding, spreading and salt tectonics is recorded concomitantly at the toe of the salt domain, as in the case of the distal Angolan passive margin (e.g. Brun & Fort 2004; Fort et al. 2004) or the Perdido fold belt in the Gulf of Mexico (e.g. Rowan et al. 2003; Jackson et al. 2010). In most of the published case studies, salt and related structures are pre-existing elements of the FTBs which are later involved in the structural evolution. However, synorogenic salt deposition is less common and has only been described in few orogenic systems, such as in the Pyrenean foreland (Vergés et al., 1992), and, more recently, in the Sivas Basin (Kergaravat et al., 2016)

The Tertiary Sivas Basin in Turkey, forming a north-directed FTB, has attracted many geologists in recent time due to its amazing outcropping conditions in addition to its potential petroleum system within the thick sedimentary accumulation (e.g. Yetiş 1968; Artan & Sestini 1971; Kurtman 1973; Gökten 1983; Gökçen & Kelling 1985; Aktimur & Tütüncü 1988; Aktimur et al. 1990; Cater et al. 1991; Yalçin & İnan 1992; Temiz et al. 1993; Guezou et al. 1996; Poisson et al. 1996; Yılmaz & Yılmaz 2006; Onal et al. 2008). Some of these studies considered the Late Eocene salt as a "classic" sedimentary layer and décollement level (Poisson et al. 1996; Temiz 1996). Apart from the work of Cubuk (1994), the importance of salt tectonics in the central part of the basin was only recently highlighted (Ringenbach et al. 2013; Callot et al. 2014; Kergaravat et al. 2016; Pichat et al. 2016; Ribes et al. 2016; Kergaravat et al. 2017; Pichat et al. 2018; Ribes et al. 2018; Legeay et al. 2018) and led to a new kinematic model of the basin in which the thick Eocene evaporites triggered the development of a large halokinetic domain, characterized by two sets of minibasins separated by a canopy.

The updated tectono-sedimentary setting of the central Sivas Basin enables now to better address the structural style of the Sivas FTB and its evolution since the Late Cretaceous. Based on the construction of 5 new balanced regional cross-sections constrained by 2D seismic profiles, we present the lateral structural variations of the Sivas Basin and discuss the influence of the stratigraphy in controlling the along-strike variability of the Sivas FTB.

GEODYNAMIC SETTING

Regional Framework

The present-day Turkey continental block is the result of the accretion of several micro-continents along the northern Eurasian active margin during the Late Cretaceous – Paleocene (Figure 1a-b-c). The closure of the Northern Neotethyan domain involved North-directed subductions and South-directed obductions evidenced by two main suture zones (Figure 1): the Izmir-Ankara-Erzincan suture zone (İAESZ), and the Bitlis-Zagros suture zone (BZSZ) (Ricou 1971; Robertson et al. 1991; Yalınız et al. 2000; Robertson 2002). A third suture, the Inner-Tauride suture Zone (ITSZ) (Figure 1) is suspected to form the trace of a hypothetic basin, in which the presence of oceanic lithosphere remains uncertain (van Hinsbergen et al. 2016; Gürer et al. 2018). Subsequent Tertiary deformation within the Anatolian microplates resulted in the formation of three major fold-and-thrust belts: the Pontides belt to the North, the Anatolides-Taurides belt between the two main sutures (van Hinsbergen et al. 2016), and the western most Bitlis-Zagros belt to the south. Late Cretaceous obduction over the Anatolides-Taurides resulted in the emplacement of ophiolites rooted along the İAESZ (Dilek et al. 1999; Yalınız & Göncüoglu 1998; Van Hinsbergen et al. 2016). The northern leading edge of the Taurides is called "Anatolides" (Kırşehir block, Tavşanlı and Afyon zone), and consists of post-obduction exhumed and metamorphosed rock units with a north to south decreasing gradient of metamorphism (Göncüoglu 1997; Okay & Tüysüz 1999; Pourteau et al. 2013; 2016). In contrast, the "Taurides" are made of non-metamorphic sedimentary rocks ranging from Palaeozoic to Cenozoic (see van Hinsbergen et al. 2016, and Gürer et al., 2018, for a geodynamic review). To the south, the Taurides are separated from the Arabian platform by the Bitlis Zagros Suture Zone (BZSZ) formed after the closure of the Southern Neotethys and Late Cretaceous obduction (e.g. Robertson et al. 2002). The collision between Anatolia and Arabia occurred during Oligocene–Miocene Times (e.g. Kaymakci et al. 2010).

The final continental collision between Arabia and Eurasia occurred most probably at Miocene time, between 20 and 10 Ma (McQuarrie & van Hinsbergen 2013). The onset of the compression resulted in the westward escape of Anatolia and in the nucleation of several NNE-SSW transtensive/transpressive faults systems in the Eastern Taurides, such as the Tecer strike-slip fault (Akyuz et al. 2013) which accommodated counterclockwise rotation of the Taurides (Gürer et al. 2018).

Anatolian Basins

The Anatolian basins along the İAESZ and the ITSZ crustal sutures developed since Late Cretaceous time (Görür et al. 1984; Görür et al. 1998). The main ones, including the Sivas Basin, are located along the southern border of the Kırşehir block while southward, other smaller sedimentary basins developed directly onto the Eastern Taurides (Figure 1a-c). These latter formed initially by back-arc extension during Late Cretaceous to Early Eocene times due to slab roll-back of the Southern Neotethys (Kaymakci et al. 2010; Robertson et al. 2012; Booth et al. 2013). The compressive phase initiated in Eocene time is associated with Southern Neotethys subduction and slab flattening between the Taurides and the Arabian plate (Darin et al. 2018), before the mature collision during Oligo-Miocene times (Agard et al. 2005; Darin et al. 2018; McQuarrie & van Hinsbergen 2013). This compression resulted in a retro-wedge development, propagating from the Bitlis-Zagros suture zone farther south into the Sivas Basin (Dhont et al. 2006; Kaymakci et al. 2010; Gürer et al. 2016; Darin et al. 2018). On a N-S transect, we can define three main supra-ophiolite depocenters, separated by basement highs, and controlled by thick-skinned structures (Figure 1a-c). The southernmost depocenter corresponds to the Hekimhan (Booth et al. 2014) and Darende Basins (Booth et al. 2013), north of the East-Anatolian orogen, bounded to the north by the south-east continuation of the Divriği ophiolitic ridge (Figure 1 a-c). The second depocenter, the Kangal Basin, is located between the Divriği and the Tecer ridges (Figure 1 a-c). The northernmost one, the Sivas Basin, is located above the ITSZ, between the Kırşehir crustal blocks and the Tecer Ridge (Figure 1 a-c).

Further west of this transect, the Sivas Basin is separated from the Ulukışla basin by the Central Anatolian Fault Zone (CAFZ) which records ~60 km of sinistral offset created during the Eocene-Oligocene times (Figure 1b) (Koçyiğit & Beyhan 1998; Jaffey & Robertson 2001). The CAFZ accommodated the shortening related to the motion of the Arabian indentor: the shortening amount in the Ulukışla Basin does not exceed 4 km (Gürer et al. 2016), whereas the Sivas Basin recorded much higher shortening as demonstrated in previous studies (Temiz et al. 1993; Guezou et al. 1996; Temiz 1996; Kergaravat et al. 2016; Legeay 2017).

Geological Framework of the Sivas Basin

The Sivas Basin exhibits no crustal extension and much more contraction than the other Tertiary Anatolian basins (Temiz et al. 1993; Guezou et al. 1996; Temiz 1996; Kergaravat et al. 2016). The Southern edge of the basin is characterized by a north-verging

thrust belt made of Maastrichtian to Eocene sediments, which is ~100 km long in the East West direction and 20 km wide from North to South (Kurtman 1973; Cater et al. 1991; Poisson et al. 1996; Gündogan et al. 2005). It is filled by shallow-water carbonates along its borders, passing to thick flysch-type deposits in the central part (Kurtman 1973; Gökten 1983; Cater et al. 1991). The upper part of the flysch succession grades to a thick evaporitic unit (Kurtman 1973; Özçelik & Altunsoy 1996; Poisson et al. 1996; Pichat 2017; Pichat et al. 2017), dated as Late Eocene (Pichat et al. 2017). This salt level was largely remobilized during the Oligo-Miocene, resulting in the formation of a salt-controlled domain in the foreland of the fold-and-thrust belt (Kergaravat et al. 2016). The core of the Sivas Basin, described as the Wall and Basin structure (WABS) by Kergaravat et al. (2016), displays a primary generation of minibasins separated by a diapiric network having spread to form a salt canopy above which developed a second generation of minibasins (e.g. Kergaravat et al. 2016; Ribes et al. 2016; Kergaravat et al. 2017; Ribes et al. 2018). The sedimentary succession of the Oligo-Miocene halokinetic domain is made of alluvial to fluvial depositional systems (Kurtman 1973; Poisson et al. 1996; Ribes et al. 2015; Ribes et al. 2016) interrupted by a regional transgression during the Late Oligocene – Early Miocene with shallow-marine deposits (Poisson et al. 2016; Ribes et al. 2018). The whole Oligo-Miocene salt domain was thrusted southward over a Late Eocene passive roof salt décollement during the regional compressive events (Kergaravat et al. 2016; Legeay 2017).

At regional scale, the Sivas Basin can be subdivided in two tectonic domains: (i) the fold-and-thrust belt (FTB) involving the Maastrichtian to Late Eocene succession, and (ii) the salt-and-thrust belt (STB) involving the Oligo-Miocene deposits and the salt-related deformations with the WABS sub-domain.

METHODOLOGY

Data from surface geology, the Celallı-1 well and seismic reflection surveys were integrated to create a regional-scale structural model and reconstruct the 3D geometry and relationships between the FTB and STB domains.

The study area (Figure 2) has a surface of 10,000 square kilometers and is covered by a 1:50.000 scale geological map recently compiled from former studies and complemented by field acquisitions in Legeay et al. (2018). The seismic reflection dataset includes fourteen 2D

seismic lines acquired in 2010-2011, provided by Transatlantic petroleum Ltd. Eleven lines are oriented NNW-SSE, perpendicular to the regional structural trend, and three lines are oriented SW-NE. The seismic data were recorded to 4000 ms two-way travel time (TWT). The Celallı-1 well was drilled in 1973 by the Mineral Research & Exploration General Directorate of Turkey in an Oligocene anticline at a total depth of 3643 m. It is the only available subsurface calibration in the area (Onal et al. 2008), used to extrapolate first order linear depth conversion of the seismic lines.

Cross-sections were built using the 2D Move © software (Midland Valley), with both seismic and surface data acquired by fieldwork. Restoration of regional cross-sections was made at first order at the top of the Eocene, prior to salt deposition, using line length conservation and flexural slip. The absence of a regional pre-kinematic marker and strong complexities in the salt domain did not allow balancing lines at the mother salt stage. The restoration is based on the minimum shortening assumption to minimize gaps between adjacent thrust sheets. Above the Eocene salt in Units 2 & 3, most of the shortening has been accommodated by the squeezing of salt ridges and diapirs, minibasins rotations and backthrusting (Kergaravat et al. 2016, 2017).

LITHOSTRATIGRAPHY & BASIN ARCHITECTURE OF THE BASIN

The used lithostratigraphic chart of the Sivas Basin was recently updated by Legeay et al. (2018) (Figure 3). A schematic cross-section (Figure 4) illustrates the first order geometry of the basin based on (i) previous studies (Guezou et al. 1996; Kergaravat et al. 2016), (ii) surface data (e.g. Legeay et al. 2018 and reference therein) and, (iii) 2D seismic profiles highlighting the main subsurface features (Figure 5).

Tectono-stratigraphy of the Sivas Basin

Five main sedimentary Groups have been identified based on work presented in Legeay et al. (2018). We briefly summarize the sedimentary content of each group in the following sections. Further detail on the sedimentary packages are available in Legeay et al. (2018) and reference therein.

Group I: Maastrichtian – Paleocene

Group I (Maastrichtian – Paleocene) consists of pre-orogenic sedimentary sequences deposited in an open marine basin (Figure 3). It first includes the Tecer Formation (750

meters-thick) consisting of Maastrichtian to Paleocene carbonate platforms, unconformably deposited on the Tauride's ophiolite along the southern edge of the basin (Kurtman 1973; İnan & İnan 1990; Cater et al. 1991). Younger Maastrichtian to Late Paleocene formations of this group include the Konakyazi, Kaleköy, Çerpaçindere and Gazibey Formations (cumulative thickness up to ~2000 meters), which are mainly composed of thick sequences of volcanoclastic and marine siliciclastic- to carbonate-rich turbiditic deposits (Gökten 1983; Aktimur et al. 1990). Note that the Çerpaçindere Formation acts as a lateral equivalent of the Konakyazi and Kaleköy Formations in the eastern part of the basin.

Group II: Eocene

Group I grades upward to the Group II around early Eocene time (Figure 3). This latter starts with the Ypresian Bahçecik Formation (700 meters-thick) outcropping on the northern and southern edges of the basin. It is made of coarse conglomerate bodies with reworked clasts sampled respectively from the (i) Kırşehir Block and Tauride margin to the north, and (ii) obducted ophiolite and Maastrichtian – Paleocene sediments to the south (Kurtman 1973). In the central part of the basin, the Bahçecik Formation laterally grades to the Kozluca Formation (500 – 600 meters-thick) corresponding to Early Eocene, thick-bedded, greenish turbidites, locally intercalated with volcanoclastic horizons (Kurtman 1973). These formations are capped by the Lutetian–Bartonian Bozbel Formation (up to 700 meters-thick) composed of thin-bedded turbidites (Artan & Sestini 1971; Kurtman 1973). Slumps and olistostromes originated from the southern fold-and-thrust-belt are locally present, especially in the western part of the basin where olistoliths can be up to 50 meters-thick. Finally, Group II ends with the evaporites of the Late Eocene Tuzhisar Formation (Figure 3) (Poisson et al. 1996; Gündogan et al. 2005; Pichat et al. 2018). When preserved from halokinetic deformation, this latter shows gyspsiferous mass transport deposits, with olistolith of gypsum and coarse to fine gypsum turbidites more or less siliciclastic-rich, interlayered with marls, and capped by a chaotic mass of porphyroblastic gypsum. The deposition of the Tuzhisar Formation is interpreted as resulting from the tectonic isolation of the basin from the oceanic domain (Gündogan et al. 2005; Pichat 2017). It is impossible to estimate the original thickness of the autochthonous evaporite layer due to its remobilization, but considering relationships between minibasins, a substantial initial thickness around 2 km is possible (see Kergaravat et al. 2017 for details).

Group III: Early Oligocene

Group III (upper Eocene to early Oligocene) is made of continental clastic deposits (Figure 3) that filled a first generation of salt-walled minibasins developed in the Tuzhisar Formation of the Group II. It involves the Selimiye Formation dominated by reddish to greenish shales, alternating with red-purple fluvial sandstones interpreted as deposited in playa-lakes and fluvial systems (Kurtman 1973; Cater et al. 1991; Gündogan et al. 2005; Onal et al. 2008). The thickness of the Selimiye Formation vary from one minibasin to another and may locally exceed 2000 m (Kergaravat et al. 2016).

Group IV: Middle Oligocene to middle Miocene

Group IV (middle Oligocene–middle Miocene) is made of continental clastic to shallow marine deposits, locally separated from Group III by allochthonous salt canopy (Figure 3). Group IV thus forms the main infill of secondary minibasins. It includes three formations: the Karayün, Karacaören and Benlikaya formations (Ribes et al. 2015; Kergaravat et al. 2016). The thickness of each formation is dependent on the amount of halokinesis and is thus variable across the different minibasins.

The Karayün Formation successively records playa-lake deposits, fluvial braided siliciclastics and saline lacustrine deposits (Ribes et al. 2015; Ribes et al. 2016). The Karacaören Formation conformably or unconformably overlies the Karayün and Selimiye formations, and locally directly lies on the salt canopy (Temiz 1996; Kergaravat et al. 2016). It consists of shallow marine marls and sandstones, locally interbedded with algal limestones dated Aquitanian-Burdigalian (Sirel et al. 2013; Poisson et al. 2016; Ribes et al. 2018). The Benlikaya Formation is characterized by alluvial to fluvial and lacustrine deposits, dated from middle to late Miocene (Poisson et al. 1996; Ribes et al. 2018). It mainly consists of reddish sandstones and conglomerates grading upward to lacustrine and sabkha evaporites (Poisson et al. 1996; Poisson et al. 2016; Pichat, 2017; Ribes et al. 2018).

Group V: Upper Miocene – Pliocene

The Group V (middle Miocene – Pliocene) mainly crops out south of the Sivas Basin, on top of the Kangal Basin, and north of the Sivas Basin in the Kizilrmak foreland. It was deposited during the last contractional stage (see Kergaravat et al. 2016; Legeay et al. 2018). The Group V includes the Incesu Formation, composed of clastic fluvial and lacustrine facies dated as late Miocene (Poisson et al. 1996), which is unconformably overlain by early Pliocene lacustrine limestones of the Merakom Formation (Guezou et al. 1996; Poisson et al. 1996).

Architecture of the Sivas Basin

The Sivas Basin can broadly be subdivided in four E-W elongated structural units, as defined along the synoptic section X-X' (Figure 4). They are characterized by common features on seismic data (Figure 5) and outcrops:

- Unit 1 (Figure 5a-b) in the south, forms the ***Sivas fold-and-thrust belt*** (FTB) and is made of north-verging thrust sheets involving pre-salt formations, i.e., the Tauride basement, the ophiolite, and Maastrichtian-Paleocene sedimentary covers (Groups I & II, Figure 3) (Kurtman 1973; Guezou et al. 1996; Temiz 1996). The FTB forms an east-west topographic ridge bounding the basin to the south, with a maximal elevation around 2800 m. Growth structures in Group II (Kozluca and Bozbel formations) can locally be recognized on field and seismic lines in this Unit (Figure 5a).

- Units 2 and 3 in the central part of the Sivas Basin (Figure 5b-c-d), form the ***salt-and-thrust belt*** (STB) with the primary (Unit 2) and secondary (Unit 3) generations of minibasins (Figure 4), bounded southward by a south-verging passive roof décollement (Figure 5b), and the north-verging Sivas Thrust to the north (Figure 5d) as defined by Poisson et al. (1996). In the Central area of the section, back-thrusts rooted along the northern pinch-out of the mother salt (Kergaravat et al. 2016) contribute to the stacking of the primary minibasins (Figure 5c).

- Unit 4 involves the stratigraphic Group V at surface, and possibly older groups at depth. It forms the preserved foreland north of the Sivas Thrust (Poisson et al. 1996) in which sediments progressively onlap the Kırşehir Block (Figure 5c).

Structural domains in Sivas Basin

Figure 6 presents two maps, one of the structural domains and one of the evaporite levels. Both help to emphasise the along strike variation of the basin architecture, and the study area is accordingly subdivided into three areas: the Western, Central and Eastern areas.

In map view, the **Western area** is rather cylindrical with an overall synclinal shape and few salt structures, diapirs and minibasins. The map shows four WSW-ENE stripes corresponding to the four structural units, separated by thrust faults and salt ridges (Figure 6a):

- **Unit 1** – Unit 1 forms a rather wide FTB thrust wedge bordered to the south by the Tecer strike-slip fault behind which outcrop the elongated Tecer syncline, filled by Oligo-Miocene deposits (Figure 4). The hinge of the wedge, made of thrusted peridotite, is exposed between the Tecer Syncline and the folded-thrust Eocene flysch in the Deliilyas area (Figure 6).
- **Unit 2** – Unit 2 is exposed as two E-W-elongated narrow bands of the Selimiye Formation bordered by diapiric evaporites. The northern band forms the Tatlicak south-dipping monocline, while the southern band displays overturned borders and is partially covered by Pliocene-Quaternary sediments (Figure 6).
- **Unit 3 –** Unit 3 forms the Savcun Syncline, an E-W-elongated minibasin filled by the Karayün Formation (Group IV) and located between the two stripes of Unit 2. Surrounding salt ridges suggest that it was deposited over an initially continuous evaporite layer over the Unit 2 (Figure 6b).
- **Unit 4** - The northernmost Unit 4 is the Kizilrmak foreland Basin (Figure 5d), north of the Sivas Thrust, a plateau of sub-horizontal continental Pliocene sediment (Group V).

The **Central area** displays a more complex organization:

- **Unit 1** - Unit 1 consists of a narrow fold-and-thrust belt involving Groups I & II along the Tecer Ridge, and bordered on its south by a wide basement exhumation (ultramafic rocks and Taurides platform) (Figure 4). This latter is locally covered by Groups II, III and IV, in the lateral continuity of the Tecer Syncline previously described in the Western area.
- **Unit 2** – Unit 2 displays the large Günduzköy minibasin (Group III), that dips 45° west over a 15 km distance (Kergaravat et al. 2016), and is unconformably onlapped by the Benlikaya Formation (Group IV). Along its southern and eastern borders, Unit 2 overthrusts the Unit 1 (Figure 2).
- **Unit 3** – Unit 3 is made of secondary minibasins filled by Group IV (the WABS province according to Kergaravat et al. 2016). The minibasins are welded, thrusted and locally wrench-faulted against each other (Kergaravat et al. 2017). A wide northern evaporitic domain, extending eastward, covers the northern half of the Unit 3.
- **Unit 4** – Unit 4 forms a narrow belt located in front the Sivas Thrust.

The **Eastern area** exhibits an architecture quite similar to the central area:

- **Unit 1** – Unit 1 is widening toward the east, structured by a system of detachment folds which turn from E-W to NW-SE around the ultramafic body of the Tecer Ridge. The FTB also locally displays an en-échelon pattern. Along its northern border, Unit 1 is overthrusted by Unit 2.
- **Unit 2** – Unit 2 shows a pattern of uplifted primary minibasins separated by squeezed salt ridges and welds. Primary minibasins are well-exposed in the center of the area, where the Unit 3 is locally absent, forming a window on Unit 2.
- **Unit 3** - In the west of the eastern domain, the extension of the WABS province, and related Unit 3, is characterized by smaller minibasins (Figure 6a). To the east, a very thick syncline with a southern monoclinal wedge of Group IV (Karayün to Benlikaya Formations) culminates at 2800 m and is called the Bey Dagi (Figure 6a, see Legeay 2017). The northern part of the eastern area, in a way similar to the central area, is covered by the northern evaporitic domain (Figure 6 b) on top of which erosional remnants of early Miocene marine limestones are found (Karacaören Formation). To the north, and above the Sivas Thrust, a ridge of evaporite forms a hectometer bulge (100 to 200 m of topography) also covered by Early Miocene deposits.
- **Unit 4** – Unit 4 once again records a narrow belt of Pliocene deposits overthrusted to the South by the Sivas Thrust. North of Unit 4, Eocene (Group II) deposits outcrop over a wide area.

STRUCTURAL STYLE OF THE SIVAS BASIN

To determine the structural style of the Sivas Basin and the amount of shortening in the three E-W areas previously defined (Figure 6a), three dip cross-sections based on seismic data were constructed (locations in Figure 2) in the western area (Figures 7 and 8), in the central area (Figures 9 and 10) and in the eastern area (Figures 11 and 12). Each of them were restored at the top of the Late Eocene Bozbel Formation. Two cross-sections along the axis of the basin were also built to illustrate the along-strike variability of structures (Figure 13). The

basement is not well imaged in the presented seismic sections. However, based on the regional maps, it is possible to extrapolate under the FTB/STB the presence of ultramafic basement to the South, and of the Kırşehir basement to the north. It is not excluded that ophiolite remnants are present onto the southern margin of the Kırşehir block below the Tertiary sediments (following the scenario of a single ophiolitic nappe from north to south).

Western area, Cross-section A (Figures 7 and 8)

The western area is represented by the seismic section a-a' (Figure 7) and the regional cross-section A-A' (Figure 8a). Seismic data highlights the cylindrical structure of the western area as shown on map view (Figure 2).

West of Ulaş, the Karacalar Anticline and surroundings are well exposed (Figure 8b), enabling to constrain the size and shape of the thrust sheets in the Late Paleocene (Kaleköy Formation) to Early Eocene (Kozluca Formation) of the FTB. The deep structures of Unit 1 remains poorly constrained but its overall shape is a thrust wedge, partly blind under the mother salt (Figure 7). Thrust sheet geometries and seismic images suggest that the associated thrusts are rooted into the Late Cretaceous sediments (lateral equivalent of the Tecer Formation, Group I), above the ophiolite. This latter does not crop out along the section, but does more to the SW and to the NE below the Tecer Formation, as shown in the Figure 8c. The taper angle of the pre-salt FTB wedge appears to be quite high as a result of antiformal stack structures within the FTB hinterland (Figure 7). Further north, the FTB terminates along the topographical boundary of the foredeep, near the northern border of the Kırşehir microcontinent. The south of the FTB is covered by an extensive narrow synform composed of Groups III-IV sediments, the Tecer Syncline. Its northern border is limited by the Tecer sinistral strike-slip fault (Akyuz et al. 2013) along which local salt-related sedimentary wedges outcrop (Figure 8e).

In the STB, the primary and secondary minibasins (Units 2 & 3), related to the mother and allochthonous salt layers, are drawn with a good degree of confidence and are well tied to surface outcrops and bedding attitudes. In Unit 2, the data delineates a southern minibasin and a large, constant thickness, and gently strained monocline (Figure 7). The large salt stocks that are exposed north and south of Unit 2 are extrapolated at depth. The upper Unit 3 is only made of the Karayün Formation and is separated from Unit 2 below by a thin

secondary salt layer, as highlighted by a small salt pillow (Figure 7). More to the south, Unit 2 is laterally limited from Unit 3 by an E-W salt ridge rooted in a canopy (Figure 8d).

At surface, the Unit 4 shows thick horizontal Pliocene deposits (Group V), thrusted by the Sivas Thrust along the northern salt ridge which is rooted within the autochthonous salt (Poisson et al. 1996). At depth, an Oligo-Miocene wedge, thinning northward, can be drawn above the pre-salt deposits. These latter seem to be affected by normal faults that may record a forebulge effect during the deposition of the Oligo-Miocene beds.

The restored cross-section at the top of the pre-salt sedimentary sequences between the Tecer Ridge and the Kizilirmak Basin shows that shortening is ~15 km (+/- 1.5 km), or 21-25% (the estimated error is ~10%).

Central area, Cross-section B (Figures 9 and 10)

The central area is represented by the seismic section b-b' (Figure 9) and the regional cross-section B-B' (Figure 10a). It exhibits the strong halokinetic pattern previously introduced in the regional setting and already studied by Kergaravat et al. (2016; 2017).

The obduction contact between the ophiolite and the Taurides limestones is exposed south of the cross-section (Figure 10 b). The contact is characterized by few meters of greenschist above limestones and, locally, the contact also shows ophiolitic mélange below the peridotite nappe (Parlak et al. 2006; Robertson et al. 2013). The ophiolite is covered along the Tecer Ridge by Maastrichtian limestones of the Tecer Formation (Kurtman 1973; İnan & İnan 1990), locally eroded and covered by patches of the Bahçecik Formation. The southern side of the Tecer Ridge is affected by several small-scale thrust sheets in which unconformable evaporites (Tuzhisar Formation) are preserved between ophiolite and Eocene clastic deposits (Figure 2 & Figure 10c). To the north of the outcropping Tecer Ridge, the seismic section reveals the stacking of thrust sheets which form the main contractional area of the FTB (Figure 9). As in the previous cross-section, the base of the Group I probably acts as the main décollement layer, which appears locally cut by thick-skinned structures rooted in the ophiolitic basement. Compressive deformation within Unit 1 seem to extend far to the North below Units 2 and 3. The FTB presents a relatively low taper angle at depth compared to the western section.

The STB occupies a wide part of the FTB, which is almost entirely covered by the evaporites. The mother salt limit is defined by strong reflections between the FTB (Unit1) and the overlying minibasins (Unit 2). To the north, the STB is limited by the Sivas Thrust

whereas to the south, it is limited by the south-verging passive-roof thrust below Unit 2, well exposed at surface (Figure 10d). The southernmost Gündüzköy primary minibasin (Unit 2) is shaped as a westward large prograding monocline depocenter forming an expulsion rollover (see Kergaravat et al. 2016) while other northern minibasins of Unit 2 are aligned until the pinch-out of the mother salt. Pinch-out is suspected to occur north of the Emirhan minibasin, where south-dipping reflectors become parallel and rather undisturbed. Minibasins of Unit 2 are covered by a large salt canopy on which several secondary minibasins of Unit 3 developed (Figure 9). The complex outcropping pattern of these secondary minibasins and salt ridges corresponds to the WABS province described by Kergaravat el al. (2016; 2017). At depth, the exact delineation of the canopy between the primary and the secondary minibasins is quite interpretative due to the poor seismic quality resulting from salt tectonics complexity. Nevertheless, the outcropping WABS domain together with the subsurface interpretations of the STB evidence a more important salt tectonics activity than in the western area (Figure 8).

North of the STB, the northern evaporitic domain is narrow and rooted to the canopy level. There, the evaporites form a salt relief at the boundary between Unit 3 and 4. This structure is interpreted as limited by the Sivas Thrust. Further south, the evaporite bulge probably records a Pliocene salt sheet having spread southward on the Benlikaya Formation on top of the Kizilkavraz minibasin (Figure 10a).

Finally, the incipient Unit 4 is deposited onto the Kırşehir basement, and appears to be narrower and thinner than in the west.

The restored cross-section at the top of the pre-salt sedimentary sequences between the Tecer Ridge and the Kizilrmak Basin show that shortening is ~20 km (+/- 2 km), or 22-27% (the estimated error is ~10%).

Eastern area, Cross-section C (Figures 11 and 12)

The eastern area is represented by the seismic section c-c’ (Figure 11) and the regional cross-section C-C’ (Figure 12a).

In the FTB, the seismic image of Unit 1 shows a thick package of high reflectivity reflectors dipping to the north, below the Late Eocene mother evaporite (Figure 11). Such geometry of Late Cretaceous to Eocene deposits (Groups I and II) contrasts with the belt of detachment folds seen at surface and in seismic further south in the same rock sequence

(Figure 2), (Figure 9). The downdip termination of the monocline shows an apparent southward toplap below the base salt. This geometry suggests the presence of a large thick-skinned anticline of peridotite below the FTB. This sedimentary package is still interpreted as being detached on a Late Cretaceous-Paleocene shaly sequence of the Çerpaçindere Formation, especially thick in this part of the basin. As in the central part, deep fold and thrust within Unit 1 seem to extend far to the North. The FTB displays an intermediate taper angle compared to the western and central sections. To the south, at the back of the FTB wedge, the Oligo-Miocene elongated depocenter (westward prolongation of the Tecer syncline) is wide and lies on the evaporites. These evaporites rest either over Nummulitic limestones and conglomerates (Bahçecik Formation) or directly over the peridotite. Halokinetic structures as well as minibasins are present there, but have not been studied in details yet.

Like in previous sections, the STB involves the Units 2 and 3 with two generations of minibasins separated by a discontinuous allochthonous salt canopy between exhumed primary minibasins. However, the canopy appears smaller than in the central part. The southern STB is decoupled from the FTB by the passive roof back-thrust which is arched and partially eroded in the southernmost part. There, two distinct primary minibasins separated by a salt diapir are recognized with a good degree of confidence, both at surface and on the seismic section. Note that, contrary to the previous sections, the marine Karacaören Formation unconformably covers and fills some of these primary minibasins, without deposition of the Karayün Formation. North of these primary minibasins, two secondary minibasins of the Unit 3 developed on the salt canopy, with large halokinetic wedges and sequences in their sedimentary infill (Group IV, Figure 12b). These two secondary minibasins on the section belong to a group of 4 scenic small secondary minibasins developed on the southern edge of the very wide northern evaporitic domain (Figure 2). These secondary minibasins are limited along the northern edge by the backthrusting of large primary minibasins. At depth, we suspect the presence of welded primary minibasins as outcropping eastward of the section (Figure 12c)

The northern-half of the STB is sealed by the extensive northern evaporitic domain. Its rugged topography resulted in poor quality seismic imaging (Figure 11), but reflectors suggest a single wide primary minibasin underneath the evaporites. Numerous hills of Lower Miocene marine limestones rest above the evaporites, evidencing the emplacement of this evaporites prior to the marine transgression. The large extension of the evaporites and their

sedimentary layering at outcrop suggest that they are not purely allochthonous, but also depositional. The evaporites likely precipitated in a large saline lake at the end or during the Karayün Formation. The ions having fed the evaporite precipitation were most probably fed by the surface to subsurface dissolution of diapirs in the central part of the STB (Pichat 2017; Pichat et al. 2018).

The northern side of the STB is fringed by a prominent relief on which the Early Miocene Günyamaç marine minibasin is preserved (Figure 12a). The relief is the sign of still active salt motion, as the present-day topographical depression between Hafik and Zara suggests actively downbuilding minibasins. The northern diapiric ridge is here presumed to be connected at depth to the mother salt layer (Figure 12a) with once again active thrusting along the Sivas Thrust.

Finally, we note that the Pliocene sediments are absent in the northern edge of the basin. However, Early Miocene limestones are deposited unconformably onto Eocene clastic units and are thrusted by the Sivas Thrust.

The restored cross-section at the top of the pre-salt sedimentary sequences between the Tecer Ridge and the Kizilrmak Basin show that shortening is ~24 km (+/- 2.4 km), or 27-33% (the estimated error is ~10%).

Cross-sections along the axis of the basin (Figure 13)

Cross-section D-D'

Cross-section D-D' cuts through the FTB (Figure 13a, location in Figure *2*) and intersects (1) the western domain, where the wedge is exposed with Eocene at surface; (2) the central domain over the Gündüzköy minibasins and the triangle zone, and (3), the eastern area, where it crosses the FTB exposed or hidden beneath the passive roof. The section allows correlating the detachment at the base of the FTB wedge in the Upper Cretaceous-Paleocene. The top ophiolite is interpreted on seismic with a lesser degree of confidence.

Cross-section E-E'

Cross-section E-E' cuts through the STB (Figure 13b, location in Figure *2*) and allows the correlation of the Units 2 and 3 with primary and secondary minibasins lying in autochthonous to allochthonous salt levels. Below the mother salt, the deformation front of the thrust wedge remains poorly imaged. The basal décollement can hardly be constrained and the Kırşehir Block and overridden ophiolite are schematically drawn. Note that along the

section E, Unit 2 exhibits thinner primary minibasins in the central area than in the East and West. Moreover, the salt canopy is absent in both edges of the line. In the eastern area, the northern salt nappe lies above the Karayün Formation. Finally, we note that the central domain is characterized by (i) minibasins filled by a thick Karayün Formation and (ii) minibasins filled by the Karacaören and Benlikaya formations which are absent on the eastern and western edges of the section (Kergaravat et al. 2016; Kergaravat et al. 2017).

SEQUENTIAL EVOLUTION OF THE SIVAS BASIN

Based on the data presented in this study and the previous kinematic study performed by Kergaravat et al. (2017) in the central halokinetic domain, we propose the following sequential evolution of the Sivas Basin synthetized in four main time steps since Maastrichtian times (Figure 14).

Maastrichtian to Eocene step from post-obduction open marine to salt deposition (Figure 14a-b)

After the emplacement of the ophiolitic nappe, several sedimentary successions deposited on its top (Figure 3), during the Late Cretaceous and Paleocene (Figure 14a): (i) the Tecer limestone forming a platform along the edge of the Anatolide-Tauride Block to the south, (ii) their basin equivalent made of deep-water turbidites and calciturbidites derived from the dismantlement of the platform, and (iii) volcanoclastics derived from possible submarine basaltic and andesitic lava flows (Konakyazi, Kaleköy, Çerpaçindere Formations) (Gökten 1983; Gökten 1986; Aktimur et al. 1990; Legeay et al. 2018). Strong post-obduction subsidence is evidenced by the deposition of up to 700 meters-thick shallow-water platform carbonates and 2000 meters-thick volcanoclastic turbidites.

During the early Eocene, the occurrence of olistostromes and mass flows derived from both the southern and northern margins of the Sivas Basin (Bahçecik Formation, Figure 3) indicate the onset of deformation and uplift along these two boundaries: onto a Paleocene karstified limestone surface along the southern border (Kurtman 1973; Cater et al. 1991), and along the İAESZ in the north (Kurtman 1973; Poisson et al. 1996). This period has been interpreted as the onset of development of the Sivas fold-and-thrust belt (Legeay et al. 2018).

The main thrusts are rooted within the ophiolite nappe and within the Late Cretaceous turbiditic formations.

From the early Eocene to the late Eocene salt deposition (Tuzhisar Formation), a relatively slow northward propagating shortening induced local growth structures in the Group II (Kozluca and Bozbel Formations, Figures 3 and 5a). Deposition of Bartonian evaporites directly on top of the anticlines constituted by ophiolitic rocks (Figure 10c) evidence the pre-salt growth of these folds along the southern boundary of the Sivas Basin (Figure 14b). Along the southern edge of the basin, the primary evaporite displays intercalated gypsum olistoliths and gypsiferous turbidites, which also support a synorogenic depositional environment (Pichat 2017). This shortening activity induced the isolation of the foreland from the oceanic domain, which allowed the deposition of thick evaporite deposits (Gündogan et al. 2005; Pichat 2017). The Tuzhisar salt deposited all over the Sivas Basin and entirely filled the foredeep (Figure 14b).

The Late Cretaceous–Paleocene sedimentary succession (Figure 3) represents the marine infill of a 60-70 km-wide flexural basin formed on top of a large southward-directed ophiolitic obduction above the continental Tauride margin. Time-equivalent shallow water carbonate platforms occurred southwards in the Hekimhan and Darende basins (Booth et al. 2013; Nairn et al. 2013; Booth et al. 2014). Although the initial shape of the basin was wide and relatively symmetric as depicted in Figure 14a-b, north-directed shortening along the Tauride boundary of the basin resulted in the folding and local thrusting of the southern Sivas Basin. This deformation occurred before the end of the Eocene period. It was triggered by the continental collision of Tauride and Arabia as proposed by Darin et al. (2018), or, alternatively, by other early tectonic processes related to initial collision. Along the southern boundary of the Sivas Basin, the large and north-directed Tecer and Divriği antiforms grew during this deformation period (see Legeay et al. in revision).

Late Eocene to middle Oligocene step of primary minibasins growth during tectonic quiescence (Figure 14c)

During the latest Eocene and the lower Oligocene (Figure 14c), salt deposition was followed by the deposition of 2.5 to 5.0 km-thick fined-grained playa-lake to fluvial deposits (Selimiye Formation, Figure 3) (Ribes et al. 2015; Kergaravat et al. 2017).

This period is characterized by the development of primary minibasins that were the driver for salt remobilization and initial salt canopy emplacement above the Selimiye Formation (Kergaravat et al. 2016, 2017). Canopy development occurred by the suturing and

coalescence of individual salt sheets, with some input from erosion and redeposition of evaporites from diapirs (see Pichat 2017). In the central area (Figures 10 and 14c), the southernmost prograding rollover in the Unit 1 (Günduzköy Minibasin) favoured a greater salt flow to the north (Figures 8 and 12).

The late Eocene to middle-Oligocene period is considered to be relatively tectonically quiet according to (i) the lack of syn-sedimentary deformation and (ii) the scarcity of coarse-grained clastic deposits. South of the Sivas Basin, Oligocene clastic sediments were not deposited or confined within the Darende and Hekimhan basins with less than 250 m of sediments (Booth et al. 2013, 2014). However, a tectonic activity can also has been inhibited by the movements of the salt and related halokinesis. Moreover, it is likely that the structural relief of the base salt, evolving during contraction, contributed to the localization of salt structures between the primary minibasins (see Dooley et al. 2018, for further details of impact of base salt relief on salt flow).

Middle Oligocene to late Miocene step of secondary minibasins growth during shortening (Figure 14d-e)

The tectono-sedimentary evolution of this period is mostly characterized by the growth of secondary minibasins in the central area of the Sivas Basin, above the salt canopy, as drawn in the Figure 14d-e (Ribes et al. 2015, 2016, 2018; Kergaravat et al. 2016, 2017).

During the deposition of the continental Karayün Formation (Figure 3, Figure 14d), three main sedimentation periods are associated to different halokinetic strata patterns: (i) a first period showing salt-related accommodation dominated by diapirism and fine grained sediments; (ii) a second period of high clastic deposition burying salt structures; and (iii) a third period during which regional shortening triggered the rejuvenation of diapiric structures by squeezing them (see Ribes et al. 2015; 2016 for details). Before the third period, the pre-salt FTB developed as a passive roof duplex before shortening record in the STB, as highlighted by diapiric growth. But despite the propagation of the deformation into the STB, the FTB kept propagating to the north at depth below the main salt décollement level. The high rate of deposition inferred for the Karayün Formation was interpreted as resulting from (i) the flexural subsidence preceding significant regional shortening and (ii) coeval salt extrusion at the end of the Oligocene (Kergaravat et al. 2016, 2017; Ribes et al. 2016).

The Chattian–Aquitanian westwards regional transgression reached the central parts of the Sivas Basin, but was not recorded further west. Several secondary minibasins were infilled by shallow-marine intermixed carbonates, delta-plain and lagoon deposits (Figure 3), composing the Karacaören Formation (Figure 14e, Poisson et al. 2016; Ribes et al. 2018). The thickest Karacaören sedimentary successions deposited in E-W trending depocenters within the central area of the STB. This repartition was the result of sustained shortening in the STB, with the progressive welding of the diapirs and their evolution into E-W oriented thrust and backthrust (Kergaravat et al. 2016, 2017; Ribes et al. 2018). Further east, the northern evaporitic domain was covered by the Karacaören marine deposits. This area thus formed the uppermost level of the canopy spreading to the north during the late Oligocene.

The regional regression during middle Miocene time is recorded in the Sivas Basin with the continental siliciclastic Benlikaya Formation deposited above the Karacaören Formation (Figure 3; Poisson et al. 1996; Ribes 2015; Ribes et al. 2018). Erosion of previous sedimentary formations and progressive exhumation of the STB and related minibasins sourced the Benlikaya Formation (Ribes et al. 2018).

Pliocene to Present step compressional step (Figure 14f-g)

The late Miocene–Pliocene fluvial and lacustrine Incesu and Merakom formations (Figure 3) mainly crop out north of the Sivas Thrust and south of the Tecer and Gürlevik ridges in the Kizilirmak and Kangal basins (Figure 2). However, it is not excluded that Pliocene deposits used to extend over a wider region in the internal Sivas Basin before recent erosion as drawn in the Figure 14f. The Sivas Thrust was still active during the Pliocene and developed in the Tuzhisar evaporites (Figure 5d), following (i) the northern limit of the original Eocene evaporites along the eastern and western regions, and (ii) the front of the salt canopy in the central part of the basin (Figure 6). To the South, the onset of movement along the Tecer strike-slip fault was related to the rotation of the Anatolian block, with the accommodation of counter clockwise rotation of the Tauride block (Gürer et al. 2018).

Southwards, the Kangal Basin (Figure1 and Figure 2) is entirely covered by late Miocene - Pliocene sediments nowadays located at higher elevations than in the Sivas Basin, highlighting that the recent N-S shortening, and related uplift, was mainly accommodated along the Sivas/Kangal basins boundary (Figure 14g).

DISCUSSION

As highlighted by the map and the cross sections, the overall geometry of the Sivas Basin is not simply cylindrical, but shows significant lateral variations of structural style, and along-strike shortening amounts varying from ~15 km to ~25 km from west to east. We hereafter discuss the origin of such an along strike variability by linking it with: (i) the basement inherited structure, (ii) the spatial and stratigraphic distribution of the main décollements, (iii) salt décollement efficiency through time and space and (iv) erosion and sedimentation.

(i) Influence of inherited structures on FTB geometry and salt tectonics

At a crustal-scale, the Kırşehir block is separated from the Taurides by the Inner-Tauride suture (Figure 1). Despite uncertainty at depth, the cross-sections show that the frontal thrust of the pre-salt FTB wedge fringes the probable southern limit edge of the Kırşehir block (Figures 8a-10a-12b). Moreover, our cross-section restorations suggest that the Kırşehir block formed a topographic high since its Late Cretaceous-Paleocene exhumation (Figure 14). We propose that the presence of this structure had a first-order impact on the structural evolution of the FTB. The Kırşehir block acted as a rigid block limiting the northward propagation of the FTB. The variable amounts of displacement restored at the top of the pre-salt (i.e. the shortening amounts varying from ~15 km to ~25 km from west to east, Figures 8a-10a-12a) are thus interpreted as a result of the progressive disappearance of the Kırşehir block, between the Pontides and the Taurides, toward the north-east end of the basin.

This interpretation is supported by the FTB geometry itself, which at first order depends on the ability of the FTB to accommodate the deformation towards the foreland (e.g. Davis et al. 1983; Dahlen et al. 1984). In the western Sivas Basin, due to the proximity of the Kırşehir block edges, propagation of shortening was hindered, resulting in a shorter FTB and an antiformal stack. Along strike to the east, the widening of the basin, outboard of the Kırşehir block, allowed an easier propagation of the FTB at depth along the bottom décollement, below the passive-roof thrust, allowing a lower taper angle of the FTB in the central and eastern areas.

Therefore, the presence of the Kırşehir block induced an edge effect in the foreland. Deformation propagated easier toward the north above basal décollement in the eastern and central area (Figures 10 and 12) compared to the western area (Figure 18). The Kırşehir block thus controlled the first order shape of the FTB (e.g. Ghani et al. 2018). However, as further discussed below, this latter was also influenced by other factors involving erosion processes and the evolution of the STB above the mother salt layer.

(ii) A multi-décollement system

The Sivas Basin offers an opportunity to study the interaction of a multi-décollement system within a thick- and thin-skinned foreland fold-and-thrust belt. We identify four décollements contributing to the deformation, from crustal to minibasin scale (Figure 4). The first basal décollement lies in the obducted serpentinized mantle to the south (in the thick-skinned domain) and ramps up in the second Maastrichtian-Paleocene décollements, which is included in the frontal wedge. The third and fourth décollements involve the two evaporite layers within the STB: the mother salt and the allochthonous canopy. These décollements, which initiated salt tectonics, are heterogeneous and responsible for a complex transmission of the shortening both upward and frontward.

The mother salt décollement covers most of the Eocene FTB, conformably on the Eocene turbidites in most places, and unconformably on the ophiolite and on inner folded turbidites south of the basin. During the deposition of the Selimiye Formation, strong halokinetic deformation occurred and formed a set of primary Oligocene minibasins, which preferentially developed in the central and eastern parts of the basin. This pattern suggests that the mother salt was significantly thinner toward the western area of the Sivas Basin. Furthermore, the northern pinch-out forms the northern buttress, where shortening above was initiated toward the foreland (i.e western section) or the hinterland (i.e. central section) as discussed in Krzywiec and Vergés (2007).

The salt canopy acted as a significant décollement level in the central area, rooting many thrusts and back-thrusts as well (Kergaravat et al. 2017). In contrast, in the eastern area, the canopy is seen as having solely controlled the local development of secondary minibasins. Eventually, in the western area, although the canopy records thrust displacement at its front, the cross-section evidences that the basalt mother salt accommodated the most important part of the compression in the STB. The rather limited extension of the salt canopy in the western and eastern area compared to the central area is once again suggesting an initially lower thickness of the mother salt both west and east of the Sivas Basin.

At a first order, we can thus describe the mechanical stratigraphy of the Sivas Basin as a dual décollement system (Figure 15a), considering it is composed of (i) an initial wedge above a frictional décollement and, (ii) a synorogenic viscous layer above this wedge on which the foreland sediments accumulated. Similar, but simpler, cases have been studied through analogue modelling (Couzens-Schultz et al. 2003; Bonini 2007; Santolaria et al. 2015). Such deformation involving synorogenic salt has also been described in natural cases (Figure 15): in the Eastern Southern Pyrenees (e.g. Krzywiec and Vergés 2007), in the Eastern Carpathian fold-thrust belt (Stefanescu et al. 2000), in the Dezful Embayment of the Zagros fold-thrust belt (Sherkati et al. 2005; Najafi et al. 2018) or in the Kuqa fold-thrust belt (Chen et al. 2004; Hubert- Ferrari et al. 2007; Zhao & Wang 2016; Izquierdo-Llavall et al. 2018). However, none of these examples ever recorded the emplacement of a salt canopy, and thus of a supplementary décollement level, as in the Sivas Basin. This difference may result from different factors involving for instance the synorogenic salt thickness or the sedimentation rates in the foreland. For a salt layer thinner than in the Sivas Basin, such as in the Southern Pyrenees belt (Figure 15b), the salt is used as a décollement level rather than as a feeder for salt structures. It allows for a good coupling between the FTB and the STB, which does not evolve separately from its deeper counterpart. Contrarily, thick mother salt allows for the building of structural heterogeneities, which will locally accommodate shortening and limits the STB 'classic' propagation like in the East Carpathian (Figure 15c) or the Dezful embayment (Figure 15d). Rapid and important sedimentation, even for initially thick salt, can inhibit salt tectonics and thus the ability to create the aforementioned ductile heterogeneities capable of buffering the shortening, favouring a good coupling between the STB and the FTB. This is clearly the case of the Kuqa fold-and-thrust belt (Figure 15e) which shows a good mechanical coupling between the pre-salt structures and the post-salt deposits although the initial salt thickness might have reached at least one kilometer (Izquierdo-Lavall et al. 2018, and references therein). Moreover, as previously discussed, the salt canopy in the Sivas Basin was partly made of depositional evaporites recycled from the mother salt at the front of salt glaciers (Pichat 2017; Pichat et al. 2018). Accordingly, the emplacement of the salt canopy in the Sivas Basin was likely resulting from a very specific combination of tectonic, climatic and sedimentological conditions that have not been reached in other foreland settings. Finally, compressive settings displaying better analogies of multi-décollement levels with coeval salt-canopy emplacement and minibasins development are rather recorded (i) in foreland basins with pre-orogenic salt deposition (e.g. the Guadalquivir

Basin, Flinch & Soto 2017) and (ii) in salt-controlled passive margin compressive toe settings (e.g. the Angola Salt Basin, Fort et al. 2004).

(iii) Influence of the salt décollement level efficiency

The mechanics of the basal décollement has a strong influence on the FTB that develops above (see Bonini 2003; Couzens-Schultz et al. 2003; Bonini 2007). The resistance of a viscous décollement level, and thus its efficiency, are at first order a product of the strain rate and the décollement level thickness (e.g. Costa & Vendeville 2002). At constant strain rate, a thin, thus resistant, upper décollement favors an in-sequence thrust-cored folds, whereas a thick and thus soft décollement favors the propagation of detachment folds (see Couzens-Schultz et al. 2003; Bonini 2007) and erratic propagation above the salt décollement (e.g. Costa and Vendeville 2002). The west and central cross sections A-A' and B-B' illustrate quite well those two end member of evolution (Figure 16a).

In the western cross section, the mother salt, relatively thin compared to the central and (to a less extend) eastern areas, developed large and few primary minibasins. Due to this configuration and synorogenic foreland sediment deposition, the rigidity of the STB was increased because few diapiric structures could accommodate shortening strains (see Callot et al. 2016; Duffy et al. 2017, 2018). In the western area, the mother salt and associated STB thus presented a relatively high resistance, which favoured the coupling with the FTB and incorporation of the STB into the FTB (Figure 16a), as highlighted in map view by the present-day regular and cylindrical structures of the western area (Figure 2). Increased resistance to foreland propagation favoured a high angle taper geometry of the FTB at the rear (favouring the stacking of thrust units) and enhanced exhumation / erosion of the FTB. Similar FTB evolution have been highlighted in the southern Pyrenees (Vergés et al. 1992; Camara & Flinch 2017) and in the Kuqa fold-thrust belt (Li et al. 2012; Izquierdo-Llavall et al. 2018, see figure 15e).

On the contrary, in the central part of the Sivas Basin, and to a lesser extent, in the eastern part, the thick initial evaporite level triggered the development of numerous small primary mini-basins limited by well-developed diapiric structures (Figure 16b). As a result, the mother salt below the STB bore almost no resistance to deformation and favoured the intracutaneous propagation of the FTB as a triangular zone. This configuration limited (i) the erosion and out of sequence development of thrusts at the rear of the pre-salt FTB, and (ii) the input of erosional products into the foreland. The propagation of the deformation across the STB was then accommodated by (i) the passive roofing, and (ii) the squeezing of the salt

structures formed during the Selimiye Formation deposition (Figure 16a) (e.g. Rowan & Vendeville 2006; Callot et al. 2012; Duffy et al. 2017).

(iv) Influence of erosion and sedimentation

Erosion and sedimentation are considered major factors controlling the shape and propagation of a foreland fold-thrust belt (e.g. Pichot & Nalpas 2009; Graveleau et al. 2012). Classically, high sedimentation rates within the foreland enhances fold building and folds and thrusts steepening (Pichot & Nalpas 2009). In the case of salt-cored thrust belts with limited allochthonous salt, a higher sedimentation rate buries the diapirs and eventually promotes the forelandward propagation of the STB in a rather rigid manner (e.g. Grelaud et al. 2002).

In the western area of the Sivas basin (Figure 16a), the basement inherited structure together with the relatively high rigidity of STB (resulting from the initially small thickness of the mother salt layer), promoted the structural uplift of the FTB at the rear of the foreland. This exhumation necessarily enhanced the erosion of the FTB and thus the sedimentation in the STB (Figure 16a). The erosion contributed to maintain the efficient exhumation of the FTB (e.g. Pichot & Nalpas 2009; Darnault et al. 2016), while the resulting sedimentation in the STB contributed to bury the diapiric structures, increasing the mechanical resistance of the overall STB (e.g. Precaspian Basin, Duffy et al. 2017; Fernandez et al. 2017). This situation kept promoting the coupling of the STB with the FTB, triggering finally (i) the forelandward propagation of thrusts and (ii) the increased uplift of the inner FTB (Figure 16a). With less halokinetic deformations than in the Sivas Basin, similar retro-action processes in the evolution of a FTB have been described in the Potwar Basin – Salt Range thrust association (Cotton & Koyi 2000; Grelaud et al. 2002), in the Southern Pyrenees (Krzywiec and Vergés 2007, Figure 15d) and in the Kuqa fold-and-thrust belt (Li et al. 2012, Izquierdo-Lavall et al. 2018, Figure 15b).

In the central, and to a lesser extent, eastern parts of the Sivas Basin (Figure 16b), the FTB and the STB kept a lower taper angle due to (i) the lower influence of the Kırşehir basement at depth, (ii) the better decoupling of the STB from the FTB (as a consequence of the thicker mother salt layer and of efficient passive roofing) and (iii) the forelandward propagation of the salt canopy. Accordingly, the STB remained relatively protected from erosion and the FTB remained hidden at depth. As a result, retro-action processes of erosion and sedimentation such as those having occurred in the western part of the basin did not occurred in the central area of the Sivas Basin.

Finally, in the eastern part of the Sivas Basin, even if the mother salt layer was initially thinner than in the central part, we suggest that the fewest number of primary mini-basins and the smaller extension of the canopy resulted from a higher sedimentation rate having limited the salt extrusion during the Selimiye Formation. This hypothesis is supported by (i) field observations of coarser clastic deposits in the eastern part of the basin compared to the central part and (ii) the westward prograding system of the Selimiye Formation, evidenced in the central part of the basin (Kergaravat et al. 2016) and highlighting thus sediments being sourced from the eastern edge of the basin.

CONCLUSION

The objectives of this study were to decipher the structure of the Sivas Basin and understand how the presence of a thick synorogenic late Eocene salt layer influenced the structural style of a fold-thrust belt. To achieve this, we combined extensive fieldwork and interpretation of a seismic dataset to construct serial upper crustal cross-sections.

1. The Sivas Basin can be subdivided into two mains thrust systems: a lower fold-and-thrust-belt and an upper salt-and-thrust belt. The fold thrust-belt is rooted in an extensive detachment level at the base of the Inner Tauride Ophiolite, and roofed by the Eocene evaporites. It includes Tauride Ophiolite unit and Late Cretaceous–Eocene sedimentary successions. It mainly developed during the middle–late Eocene period with north verging thrusts, some of which are rooted in a second decollement level in the Maastrichian-Paleocene marls.

2. The salt-and-thrust-belt is rooted in the Eocene evaporites and involves younger sediments associated with halokinetic deformations developed in the central part of the Sivas Basin during the Oligo-Miocene foreland infill. The halokinetic domain is especially marked by two generations of mini-basins separated by a salt canopy, which acted as a more restricted and shallower fourth detachments level rooting many thrusts and back-thrusts.

3. The map and the cross sections evidence that the Sivas fold-belt exhibits strong lateral variations of structural style, with a shortening that decreases progressively from 25 km in the East to 15 km in the West.

4. The Sivas fold-belt architecture and shortening was at first order influenced by the geometry of the crustal Kirshehir block which, westward, significantly limited the northward propagation of the deformation and promoted the structural uplift of the fold-and-thrust-belt through antiformal stack.

5. The coupling between the fold-and-thrust-belt and the salt-and-thrust-belt also controlled the kinematic evolution of the Sivas folded belt and varied with the thickness variation of the Eocene salt. West of the basin, efficient coupling in response to a thin salt level resulted in a classic forelandward propagation of the thrust system and a generalized behaviour of the Sivas belt as a critical taper. In contrast, in the central part and eastern part of the basin, efficient decoupling due to a thick synorogenic salt level allowed the propagation of the fold thrust-belt below the detached salt thrust-belt, which was thrusted forelandwards and backwards.

6. Westward and eastward, the coupling of the salt-and-thrust-belt with the fold-and-thrust-belt was also promoted by (i) the exhumation, erosion and re-sedimentation of the fold-and-thrust-belt at the western part of the basin and (ii) a higher sedimentation rate at the early Oligocene in the eastern part of the Sivas Basin.

7. The Sivas Basin display worldclass outcrops and stands out from other halokinetic foreland basins by its complex geological setting and its intensive synorogenic salt tectonics, marked by large canopy and two generations of minibasins.

Acknowledgments

This work results from a research agreement between TOTAL and the University of Pau (France). We thank Petroleum Transatlantic Ltd for permission to use and display the seismic data. H. Temiz and Gokhan Calinak from the Cümhuriyet University of Sivas are warmly thanked for support and collaboration during the fieldwork. A. Poisson is warmly thanked for sharing knowledge of the Sivas Basin. J. Letouzey is thanked for fruitful discussions. We are grateful to C. Bonnel, G. Hoareau, C. Ribes and B. Rouby for their contributions during field trip in understanding the region. M. Ford is warmly thanked for fruitful comments. We finally acknowledge the Volume Editor, Gonzalo Zamora, and

reviewers Tim Dooley and Piotr Krzywiec, for suggestions and comments that significantly improved the manuscript.

REFERENCES

Agard, P., Omrani, J., Jolivet, L. & Mouthereau, F. 2005. Convergence history across Zagros (Iran): constraints from collisional and earlier deformation. *International journal of earth sciences*, 94, 401-419.

Aktimur, T. 1988. 1/100.000 Ölçekli Açınsama Nitelikli Türkiye Jeoloji Haritaları Serisi Sivas-F24 Paftası (l/100.000 Scaled Geological Map Series of Turkey-Sivas F-24 Sheet). *MTA Genel Müdürlügü (General Directorate of Mineral Research and Exploration, Turkey)*.

Aktimur, H. & Tütüncü, K. 1988. 1/100.000 Ölçekli Açınsama Nitelikli Türkiye Jeoloji Haritaları Serisi Divrigi-F25 Paftası (l/100.000 Scaled Geological Map Series of Turkey-Divrig iF-25 Sheet). *MTA Genel Müdürlügü (General Directorate of Mineral Research and Exploration, Turkey)*.

Aktimur, H.T., Tekirli, M.E. & Yurdakul, M.E. 1990. Geology of the Sivas-Erzincan Tertiary basin. *Bulletin of the Mineral Research and Exploration Institute of Turkey, Ankara*, 111, 21-30.

Akyuz, H.S., Ucarkus, G., Altunel, E., Dogan, B. & Dikbas, A. 2013. Paleoseismological investigations on a slow-moving active fault in central Anatolia, Tecer Fault, Sivas. *Annals of Geophysics*, 55 (5), 847-857.

Artan, U. & Sestini, G. 1971. Geology of the Beypinari-Karababa area (Sivas province). *Bulletin Mineral Research and Exploration (Ankara, Turkey)*, 76, 72-89.

Atabey, E. & Aktimur, H. 1997. 1/100 000 Ölçekli Açınsama Nitelikli Türkiye Jeoloji Haritaları Serisi Sivas-G 24 Paftası (1/100.000 scaled geological map of Turkey-Sivas G24 section). *MTA Genel Müdürlügü (General Directorate of Mineral Research and Exploration, Turkey)*.

Barbeau, D. 2003. A flexural model for the Paradox Basin: implications for the tectonics of the Ancestral Rocky Mountains. *Basin Research*, 15, 97-115.

Beaumont, C., Fullsack, P. & Hamilton, J. 1992. Erosional control of active compressional orogens *Thrust tectonics*. Springer, 1-18.

Berástegui, X., Banks, C., Puig, C., Taberner, C., Waltham, D. & Fernández, M. 1998. Lateral diapiric emplacement of Triassic evaporites at the southern margin of the Guadalquivir Basin, Spain. *Geological Society, London, Special Publications*, 134, 49-68.

Bingöl, E. 1989. 1: 2 000 000 scale geological map of Turkey. *Publication of the Mineral Research and Exploration (MTA) of Turkey, Ankara*.

Bonini, M. 2003. Detachment folding, fold amplification, and diapirism in thrust wedge experiments. *Tectonics*, 22 (6), 1065 - 1076.

Bonini, M. 2007. Deformation patterns and structural vergence in brittle–ductile thrust wedges: an additional analogue modelling perspective. *Journal of Structural Geology*, 29, 141-158.

Booth, M.G., Robertson, A.H., Tasli, K. & İnan, N. 2014. Late Cretaceous to Late Eocene Hekimhan Basin (Central Eastern Turkey) as a supra-ophiolite sedimentary/magmatic basin related to the later stages of closure of Neotethys. *Tectonophysics*, 635, 6-32.

Booth, M.G., Robertson, A.H., Tasli, K., İnan, N., Ünlügenç, U.C. & Vincent, S. 2013. Two-stage development of the Late Cretaceous to Late Eocene Darende Basin: implications for closure of Neotethys in central eastern Anatolia (Turkey). *Geological Society, London, Special Publications*, 372, 385-419.

Brun, J.-P. & Fort, X. 2004. Compressional salt tectonics (Angolan margin). *Tectonophysics*, 382, 129-150.

Butler, R.W., Coward, M.P., Harwood, G.M. & Knipe, R.J. 1987. Salt control on thrust geometry, structural style and gravitational collapse along the Himalayan mountain front in the Salt Range of northern Pakistan. *Dynamical geology of salt and related structures. Academic Press, London*, 339-418.

Callot, J.-P., Trocmé, V., Letouzey, J., Albouy, E., Jahani, S. & Sherkati, S. 2012. Pre-existing salt structures and the folding of the Zagros Mountains. *Geological Society, London, Special Publications*, 363, 545-561.

Callot, J.-P., Jahani, S. & Letouzey, J. 2007. The role of pre-existing diapirs in fold and thrust belt development. *Thrust belts and foreland basins*, 309-325.

Callot, J.-P., Ribes, C., Kergaravat, C., Bonnel, C., Temiz, H., Poisson, A., Vrielynck, B., Salel, J.F*., et al.* 2014. Salt tectonics in the Sivas basin (Turkey): crossing salt walls and minibasins. *Bulletin de la Societe Geologique de France*, 185, 33-42.

Candan, O., Çetinkaplan, M., Oberhänsli, R., Rimmelé, G., & Akal, C., 2005. Alpine high-P/low-T metamorphism of the Afyon Zone and implications for the metamorphic evolution of Western Anatolia, Turkey. *Lithos*, 84, 102-124.

Cater, J., Hanna, S., Ries, A., & Turner, P., 1991. Tertiary evolution of the Sivas Basin, central Turkey. *Tectonophysics*, 195, 29-46.

Cemen, I., Göncüoglu, M.C., & Dirik, K., 1999. Structural evolution of the Tuzgölü basin in Central Anatolia, Turkey. *The Journal of Geology*, 107, 693-706.

Chen, S., Tang, L., Jin, Z., Jia, C., & Pi, X., 2004. Thrust and fold tectonics and the role of evaporites in deformation in the Western Kuqa Foreland of Tarim Basin, Northwest China. *Marine and Petroleum Geology*, 21, 1027-1042.

Costa, E., & Vendeville, B., 2002. Experimental insights on the geometry and kinematics of fold-and-thrust belts above weak, viscous evaporitic décollement. *Journal of Structural Geology*, 24, 1729-1739.

Cotton, J.T., & Koyi, H.A., 2000. Modeling of thrust fronts above ductile and frictional detachments: Application to structures in the Salt Range and Potwar Plateau, Pakistan. *Geological Society of America Bulletin*, 112, 351-363.

Couzens-Schultz, B.A., Vendeville, B.C., & Wiltschko, D.V., 2003. Duplex style and triangle zone formation: insights from physical modeling. *Journal of Structural Geology*, 25, 1623-1644.

Çubuk, Y. (1994) Bogazören (Imranli) Ve Karayün (Hafik) Yörelerinde (Sivas Dogusu) Yüzeyleyen Miyosen Yasli Birimlerin Tektonostratigrafisi. Doctoral Thesis, Cumhuriyet University, Sivas, Turkey, Fen Bilimteri Enstütüsü, Jeoloji Mühendisligi Anabilim Dali.

Dahlen, F., Suppe, J., & Davis, D., 1984. Mechanics of fold-and-thrust belts and accretionary wedges: Cohesive Coulomb theory. *Journal of Geophysical Research: Solid Earth*, 89, 10087-10101.

Darnault, R., Callot, J.-P., Ballard, J.-F., Fraisse, G., Mengus, J.-M., & Ringenbach, J.-C., 2016. Control of syntectonic erosion and sedimentation on kinematic evolution of a multidecollement fold and thrust zone: Analogue modeling of folding in the southern subandean of Bolivia. *Journal of Structural Geology*, 89, 30-43.

Davis, D., Suppe, J., & Dahlen, F., 1983. Mechanics of fold-and-thrust belts and accretionary wedges. *Journal of Geophysical Research: Solid Earth*, 88, 1153-1172.

Davis, D.M., & Engelder, T., 1985. The role of salt in fold-and-thrust belts. *Tectonophysics*, 119, 67-88.

Dhont, D., Chorowicz, J., & Luxey, P., 2006. Anatolian escape tectonics driven by Eocene crustal thickening and Neogene–Quaternary extensional collapse in the eastern Mediterranean region. *Geological Society of America Special Papers*, 409, 441-462.

Dilek, Y., Thy, P., Hacker, B., & Grundvig, S., 1999. Structure and petrology of Tauride ophiolites and mafic dike intrusions (Turkey): Implications for the Neotethyan ocean. *Geological Society of America Bulletin*, 111, 1192-1216.

Dooley, T. P., Hudec, M. R., Pichel, L. M., & Jackson, M. P. (2018). The impact of base-salt relief on salt flow and suprasalt deformation patterns at the autochthonous, paraautochthonous and allochthonous level: insights from physical models. In K. R. McClay and J. A. Hammerstein eds. Passive Margins: Tetonics, Sedimentation and Magmatism.*Geological Society, London, Special Publications*, *476*, SP476-13. Doi: 10.1144/SP476.13

Duffy, O. B., Dooley, T. P., Hudec, M. R., Jackson, M. P., Fernandez, N., Jackson, C. A., & Soto, J. I. (2018). Structural evolution of salt-influenced fold-and-thrust belts: A synthesis and new insights from basins containing isolated salt diapirs. *Journal of Structural Geology*, *114*, 206-221.

Duffy, O. B., Fernandez, N., Hudec, M. R., Jackson, M. P., Burg, G., Dooley, T. P., & Jackson, C. A. L. (2017). Lateral mobility of minibasins during shortening: Insights from the SE Precaspian Basin, Kazakhstan. *Journal of Structural Geology*, *97*, 257-276.

Feng, L., Bartholomew, M. J., & Choi, E. (2015). Spatial arrangement of décollements as a control on the development of thrust faults. *Journal of Structural Geology*, *75*, 49-59.

Fernandez, N., Duffy, O. B., Hudec, M. R., Jackson, M. P., Burg, G., Jackson, C. A. L., & Dooley, T. P. (2017). The origin of salt-encased sediment packages: Observations from the SE Precaspian Basin (Kazakhstan). *Journal of Structural Geology*, *97*, 237-256.

Fillon, C., Huismans, R.S., & van der Beek, P., 2013. Syntectonic sedimentation effects on the growth of fold-and-thrust belts. *Geology*, 41, 83-86.

Flinch, J. F., & Soto, J. I. (2017). Allochthonous Triassic and Salt Tectonic Processes in the Betic-Rif Orogenic Arc. In *Permo-Triassic Salt Provinces of Europe, North Africa and the Atlantic Margins,* 417-446.

Ford, M., 2004. Depositional wedge tops: interaction between low basal friction external orogenic wedges and flexural foreland basins. *Basin Research*, 16, 361-375.

Fort, X., Brun, J.-P., & Chauvel, F., 2004. Salt tectonics on the Angolan margin, synsedimentary deformation processes. *AAPG bulletin*, 88, 1523-1544.

Ghani, H., Zeilinger, G., Sobel, E. R., & Heidarzadeh, G. (2018). Structural variation within the Himalayan fold and thrust belt: A case study from the Kohat-Potwar Fold Thrust Belt of Pakistan. *Journal of Structural Geology*, *116*, 34-46.

Gökçen, S.L., & Kelling, G., 1985. Oligocene deposits of the Zara-Hafik region (Sivas, Central Turkey): evolution from storm-influenced shelf to evaporitic basin. *Geologische Rundschau*, 74, 139-153.

Gökten, E., 1983. Şarkışla (Sivas) güney-güneydoğusunun stratigrafisi ve jeolojik evrimi [Stratigraphy and geological evolution of the southsoutheast of Şarkışla]. *Türkiye Jeoloji Kurumu Bülteni*, 26, 167-176.

Gökten, E., 1986. Paleocene carbonate turbidites of the Şarkişla region, Turkey—their significance in an orogenic basin. *Sedimentary Geology*, 49, 143-165.

Göncüoglu, M., 1997. Distribution of Lower Paleozoic rocks in the Alpine terranes of Turkey. *Early Paleozoic in NW Gondwana*, 3, 13-23.

Görür, N., Tüysüz, O., & Celal Şengör, A., 1998. Tectonic evolution of the central Anatolian basins. *International Geology Review*, 40, 831-850.

Görür, N., Oktay, F., Seymen, I., & Şengör, A., 1984. Palaeotectonic evolution of the Tuzgölü basin complex, Central Turkey: sedimentary record of a Neo-Tethyan closure. *Geological Society, London, Special Publications*, 17, 467-482.

Graveleau, F., & Dominguez, S., 2008. Analogue modelling of the interaction between tectonics, erosion and sedimentation in foreland thrust belts. *Comptes Rendus Geoscience*, 340, 324-333.

Grelaud, S., Sassi, W., de Lamotte, D.F., Jaswal, T., & Roure, F., 2002. Kinematics of eastern Salt Range and South Potwar basin (Pakistan): a new scenario. *Marine and Petroleum Geology*, 19, 1127-1139.

Guezou, J.-C., Temiz, H., Poisson, A., & Gürsoy, H., 1996. Tectonics of the Sivas basin: The Neogene record of the Anatolian accretion along the inner Tauric suture. *International Geology Review*, 38, 901-925.

Gündogan, I., Önal, M., & Depçi, T., 2005. Sedimentology, petrography and diagenesis of Eocene–Oligocene evaporites: the Tuzhisar Formation, SW Sivas Basin, Turkey. *Journal of Asian Earth Sciences*, 25, 791-803.

Gürer, D., Hinsbergen, D.J., Matenco, L., Corfu, F. & Cascella, A., 2016. Kinematics of a former oceanic plate of the Neotethys revealed by deformation in the Ulukışla basin (Turkey). *Tectonics*, 35, 2385-2416.

Gürer, D., Van Hinsbergen, D.J., Özkaptan, M., Creton, I., Koymans, M.R., Cascella, A., & Langereis, C.G., 2018. Paleomagnetic constraints on the timing and distribution of Cenozoic rotations in Central and Eastern Anatolia. *Solid Earth*, 9, 295-322.

Hardy, S., Duncan, C., Masek, J., & Brown, D., 1998. Minimum work, fault activity and the growth of critical wedges in fold and thrust belts. *Basin Research*, 10, 365-373.

Harrison, J., & Jackson, M., 2014. Exposed evaporite diapirs and minibasins above a canopy in central Sverdrup Basin, Axel Heiberg Island, Arctic Canada. *Basin Research*, 26, 567-596.

Hubert-Ferrari, A., Suppe, J., Gonzalez-Mieres, R. & Wang, X. 2007. Mechanisms of active folding of the landscape (southern Tian Shan, China). *Journal of Geophysical Research: Solid Earth*, 112.

İnan, S. & İnan, N., 1990. The features of Gürlevik limestone and a newly suggested name in Tecer formation. *Bulletin of Turkish Geological Society*, 33, 51-56.

Izquierdo-Llavall, E., Roca, E., Xie, H., Pla, O., Muñoz, J. A., Rowan, M. G., ... & Huang, S. 2018. Influence of Overlapping décollements, Syntectonic Sedimentation, and Structural Inheritance in the Evolution of a Contractional System: The Central Kuqa Fold-and-Thrust Belt (Tian Shan Mountains, NW China). *Tectonics*, *37*(8), 2608-2632.

Jackson, M., & Harrison, J. 2006. An allochthonous salt canopy on Axel Heiberg Island, Sverdrup Basin, Arctic Canada. *Geology*, 34, 1045-1048.

Jackson, M., Hudec, M. & Dooley, T. 2010. Some emerging concepts in salt tectonics in the deepwater Gulf of Mexico: intrusive plumes, canopy-margin thrusts, minibasin triggers and allochthonous fragments. *Geological Society, London, Petroleum Geology Conference series*. Geological Society of London, 899-912.

Jaffey, N. & Robertson, A.H. 2001. New sedimentological and structural data from the Ecemiş Fault Zone, southern Turkey: implications for its timing and offset and the Cenozoic tectonic escape of Anatolia. *Journal of the Geological Society*, 158, 367-378.

Jahani, S., Callot, J.P., Letouzey, J. & Frizon de Lamotte, D. 2009. The eastern termination of the Zagros Fold-and-Thrust Belt, Iran: Structures, evolution, and relationships between salt plugs, folding, and faulting. *Tectonics*, 28.

Kaymakci, N., Inceöz, M., Ertepinar, P. & Koç, A. 2010. Late Cretaceous to recent kinematics of SE Anatolia (Turkey). *Geological Society, London, Special Publications*, 340, 409-435.

Kergaravat, C., Ribes, C., Legeay, E., Callot, J.-P., Kavak, K. & Ringenbach, J.-C. 2016. Minibasins and salt canopy in foreland fold-and-thrust belts: The central Sivas Basin, Turkey. *Tectonics*, 35, 1342-1366.

Kergaravat, C., Ribes, C., Callot, J.P., & Ringenbach, J.C. 2017. Tectono-stratigraphic evolution of salt-controlled minibasins in a fold and thrusts belt, the Oligo-Miocene Sivas Basin, Turkey. *Journal of Structural Geology*, 102, 75-97.

Koçyiğit, A. & Beyhan, A. 1998. A new intracontinental transcurrent structure: the Central Anatolian Fault Zone, Turkey. *Tectonophysics*, 284, 317-336.

Krzywiec, P. & Vergés, J. 2007. Role of the foredeep evaporites in wedge tectonics and formation of triangle zones: comparison of the Carpathian and Pyrenean thrust fronts. *Thrust Belts and Foreland Basins*, 385-396.

Kurtman, F. 1973. Geologic and tectonic structure of the Sivas - Hafik - Zara and Imranli Region. *Bulletin Mineral Research and Exploration (Ankara, Turkey)*, 80, 1-32.

Lacombe, O. & Bellahsen, N. 2016. Thick-skinned tectonics and basement-involved fold–thrust belts: insights from selected Cenozoic orogens. *Geological Magazine*, 153, 763-810.

Laubscher, H. 1972. Some overall aspects of Jura dynamics. *American Journal of Science*, 272, 293-304.

Legeay, E. 2017. Géodynamique du Bassin de Sivas (Turquie) - De la fermeture d'un domaine océanique à la mise en place d'un avant-pays salifère. *PhD Thesis (University of Pau, France)*.

Legeay, E., Mohn, G., Ringenbach, J.-C., Callot, J.-P., Ulianov, A. & Kavak, K. in revision. The pre- to post-obduction evolution of the Sivas ophiolite (Turkey) and implications for the pre-collisional history of Eastern Anatolia). *Tectonics*.

Legeay, E., Pichat, A., Kergaravat, C., Ribes, C., Callot, J.-P., Ringenbach, J.C., Bonnel, C., Hoareau, G., *et al.* 2018. Geology of the Central Sivas Basin (Turkey). *Journal of Maps*, 1-12.

Letouzey, J., Colletta, B., Vially, R. & Chermette, J. 1995. Evolution of salt-related structures in compressional settings. *in* M. P. A. Jackson, D. G. Roberts, and S. Snelson, eds., Salt tectonics: a global perspective: *AAPG Memoir,* 65, 41-60.

Li, J., Webb, A.A.G., Mao, X., Eckhoff, I., Colón, C., Zhang, K., Wang, H., Li, A., *et al.* 2014. Active surface salt structures of the western Kuqa fold-thrust belt, northwestern China. *Geosphere*, 10, 1219-1234.

MacKay, P. A., Varsek, J. L., Kubli, T. E., Dechesne, R. G., Newson, A. C., & Reid, J. P. 1996. Triangle zones and tectonic wedges: An introduction. *Bulletin of Canadian Petroleum Geology*, *44*(2), I-1.

McQuarrie, N. & van Hinsbergen, D.J. 2013. Retrodeforming the Arabia-Eurasia collision zone: Age of collision versus magnitude of continental subduction. *Geology*, 41, 315-318.

Mouthereau, F., Watts, A.B. & Burov, E. 2013. Structure of orogenic belts controlled by lithosphere age. *Nature geoscience*, 6, 785-789.

Mugnier, J., Baby, P., Colletta, B., Vinour, P., Bale, P. & Leturmy, P. 1997. Thrust geometry controlled by erosion and sedimentation: A view from analogue models. *Geology*, 25, 427-430.

Nairn, S.P., Robertson, A.H., Ünlügenç, U.C., Tasli, K. & İnan, N. 2013. Tectonostratigraphic evolution of the Upper Cretaceous–Cenozoic central Anatolian basins: an integrated study of diachronous ocean basin closure and continental collision. *Geological Society, London, Special Publications*, 372, 343-384.

Najafi, M., Vergés, J., Etemad-Saeed, N., & Karimnejad, H. R. (2018). Folding, thrusting and diapirism: Competing mechanisms for shaping the structure of the north Dezful Embayment, Zagros, Iran. *Basin Research*, *30*(6), 1200-1229.

Okay, A.I. 2008. Geology of Turkey: a synopsis. *Anschnitt*, 21, 19-42.

Okay, A.I. & Tüysüz, O. 1999. Tethyan sutures of northern Turkey. *Geological Society, London, Special Publications*, 156, 475-515.

Onal, K.M., Buyuksarac, A., Aydemir, A. & Ates, A. 2008. Investigation of the deep structure of the Sivas Basin (innereast Anatolia, Turkey) with geophysical methods. *Tectonophysics*, 460, 186-197.

Özçelik, O. & Altunsoy, M. 1996. Clastic petrofacies, provenance and organic facies of the Bozbel Formation (Lutetian) in the Eastern Sivas Basin (Turkey). *Marine and Petroleum Geology*, 13, 493-501.

Özgül, N. 1984. Stratigraphy and tectonic evolution of the Central Taurides. *Geology of the Taurus belt*, 77-90.

Parlak, O., Yılmaz, H. & Boztuğ, D. 2006. Origin and tectonic significance of the metamorphic sole and isolated dykes of the Divriği ophiolite (Sivas, Turkey): evidence for slab break-off prior to ophiolite emplacement. *Turkish Journal of Earth Sciences*, 15, 25-45.

Parlak, O., Karaoğlan, F., Rızaoğlu, T., Klötzli, U., Koller, F. & Billor, Z. 2013. U–Pb and 40 Ar–39 Ar geochronology of the ophiolites and granitoids from the Tauride belt: implications for the evolution of the Inner Tauride suture. *Journal of Geodynamics*, 65, 22-37.

Pfiffner, O.A. 2006. Thick-skinned and thin-skinned styles of continental contraction. *Geological Society of America Special Papers*, 414, 153-177.

Pichat, A. 2017. Dynamique des systèmes évaporitiques d'un bassin d'avant-pays salifère et processus diagénétiques associés au contexte halocinétique : exemple du bassin de Sivas en Turquie. *PhD Thesis (University of Pau, France)*.

Pichat, A., Callot, J.-P. & Ringenbach, J.-C. 2016. Diagenesis of Oligocene continental sandstones in salt-walled mini-basins—Sivas Basin, Turkey. *Sedimentary Geology*, 339, 13-31.

Pichat, A., Hoareau, G., Callot, J.P., Legeay, E., Kavak, K.S., Révillon, S., Parat, C. & Ringenbach, J.C. 2018. Evidence of multiple evaporite recycling processes in a salt-tectonic context, Sivas Basin, Turkey. *Terra Nova*, 30, 40-49.

Pichot, T. & Nalpas, T. 2009. Influence of synkinematic sedimentation in a thrust system with two decollement levels; analogue modelling. *Tectonophysics*, 473, 466-475.

Poisson, A., Guezou, J.-C., Ozturk, A., İnan, S., Temiz, H., Gürsöy, H., Kavak, K. & Özden, S. 1996. Tectonic setting and evolution of the Sivas Basin, central Anatolia, Turkey. *International Geology Review*, 38, 838-853.

Poisson, A., Vrielynck, B., Wernli, R., Negri, A., Bassetti, M.-A., Büyükmeriç, Y., Özer, S., Guillou, H.*, et al.* 2016. Miocene transgression in the central and eastern parts of the Sivas Basin (Central Anatolia, Turkey) and the Cenozoic palaeogeographical evolution. *International Journal of Earth Sciences*, 105, 339-368.

Pourteau, A., Oberhänsli, R., Candan, O., Barrier, E. & Vrielynck, B. 2016. Neotethyan closure history of western Anatolia: a geodynamic discussion. *International Journal of Earth Sciences*, 105, 203-224.

Pourteau, A., Sudo, M., Candan, O., Lanari, P., Vidal, O. & Oberhänsli, R. 2013. Neotethys closure history of Anatolia: insights from 40Ar–39Ar geochronology and P–T estimation in high-pressure metasedimentary rocks. *Journal of Metamorphic Geology*, 31, 585-606.

Raup, O.B. & Hite, R.J. 1992. *Lithology of evaporite cycles and cycle boundaries in the upper part of the Paradox Formation of the Hermosa Group of Pennsylvanian age in the Paradox Basin, Utah and Colorado*. US Department of the Interior, US Geological Survey.

Ribes, C. 2015. *Interaction entre la tectonique salifère et la sédimentation dans des mini-bassins: Exemple de l'Oligo-Miocène du bassin de Sivas, Turquie.* PhD Thesis (University of Pau, France).

Ribes, C., Kergaravat, C., Bonnel, C., Crumeyrolle, P., Callot, J.-P., Poisson, A., Temiz, H. & Ringenbach, J.-P. 2015. Fluvial sedimentation in a salt-controlled mini-basin: stratal patterns and facies assemblages, Sivas Basin, Turkey. *Sedimentology*, 62, 1513-1545.

Ribes, C., Lopez, M., Kergaravat, C., Crumeyrolle, P., Poisson, A., Callot, J.-P., Paquette, J.-L. & Ringenbach, J.-C. 2018. Facies partitioning and stratal pattern in salt-controlled marine to continental mini-basins: Examples from the late Oligocene to early Miocene of the Sivas Basin, Turkey. *Marine and Petroleum Geology*.

Ribes, C., Kergaravat, C., Crumeyrolle, P., Lopez, M., Bonnel, C., Poisson, A., Kavak, K.S., Callot, J.-P.*, et al.* 2016. Factors controlling stratal pattern and facies distribution of fluvio-lacustrine sedimentation in the Sivas mini-basins, Oligocene (Turkey). *Basin Research*, vol. 29, 596-621.

Ricou. 1971. Le croissant ophiolitique péri-arabe: Une ceinture de nappes mises en place au crétacé supérieur. *Géographie Phys. et Géologie Dynam*, 13, 327-349.

Ringenbach, J.-C., Salel, J.-F., Kergaravat, C., Ribes, C., Bonnel, C. & Callot, J.-P. 2013. Salt tectonics in the Sivas Basin, Turkey: outstanding seismic analogues from outcrops. *first break*, 31, 93-101.

Robertson, A.H.F. 2002. Overview of the genesis and emplacement of Mesozoic ophiolites in the Eastern Mediterranean Tethyan region. *Lithos*, 65, 1-67.

Robertson, A.H.F., Parlak, O. & Ustaömer, T. 2012. Overview of the Palaeozoic–Neogene evolution of Neotethys in the Eastern Mediterranean region (southern Turkey, Cyprus, Syria). *Petroleum Geoscience*, 18, 381-404.

Robertson, A.H.F., Clift, P., Degnan, P. & Jones, G. 1991. Palaeogeographic and palaeotectonic evolution of the Eastern Mediterranean Neotethys. *Palaeogeography, Palaeoclimatology, Palaeoecology*, 87, 289-343.

Robertson, A.H.F., Parlak, O., Metin, Y., Vergili, Ö., Tasli, K., İnan, N. & Soycan, H. 2013. Late Palaeozoic–Cenozoic tectonic development of carbonate platform, margin and oceanic units in the Eastern Taurides, Turkey. *Geological Society, London, Special Publications*, 372, 167-218.

Rowan, M.G., Lawton, T.F., Giles, K.A. & Ratliff, R.A. 2003. Near-salt deformation in La Popa basin, Mexico, and the northern Gulf of Mexico: A general model for passive diapirism. *AAPG bulletin*, 87, 733-756.

Rowan, M.G., Ratliff, R.A., 2012. Cross-section restoration of salt-related deformation: Best practices and potential pitfalls. J. Struct. Geol. 41, 24–37. doi:10.1016/j.jsg.2011.12.012

Rowan, M. G., & Vendeville, B. C. (2006). Foldbelts with early salt withdrawal and diapirism: Physical model and examples from the northern Gulf of Mexico and the Flinders Ranges, Australia. *Marine and Petroleum Geology*, *23*(9-10), 871-891.

Santolaria, P., Vendeville, B.C., Graveleau, F., Soto, R. & Casas-Sainz, A. 2015. Double evaporitic décollements: Influence of pinch-out overlapping in experimental thrust wedges. *Journal of Structural Geology*, 76, 35-51.

Şengör, A. & Yılmaz, Y. 1981. Tethyan evolution of Turkey: a plate tectonic approach. *Tectonophysics*, 75, 181-241.

Sherkati, S., Letouzey, J. & Frizon de Lamotte, D. 2006. Central Zagros fold-thrust belt (Iran): New insights from seismic data, field observation, and sandbox modeling. *Tectonics*, 25.

Sherkati, S., Molinaro, M., de Lamotte, D.F. & Letouzey, J. 2005. Detachment folding in the Central and Eastern Zagros fold-belt (Iran): salt mobility, multiple detachments and late basement control. *Journal of Structural Geology*, 27, 1680-1696.

Sirel, E., Ozgen Erdem, N. & Kangal, O. 2013. Systematics and biostratigraphy of Oligocene (Rupelian-Early Chattian) foraminifera from lagoonal-very shallow water limestone in the eastern Sivas Basin (central Turkey). *Geologia Croatica*, 66, 83-110.

Stefanescu, M., Dicea, O. & Tari, G. 2000. Influence of extension and compression on salt diapirism in its type area, East Carpathians Bend area, Romania. *Geological Society, London, Special Publications*, 174, 131-147.

Talbot, C. & Alavi, M. 1996. The past of a future syntaxis across the Zagros. *Geological Society, London, Special Publications*, 100, 89-109.

Temiz, H. 1996. Tectonostratigraphy and thrust tectonics of the central and eastern parts of the Sivas Tertiary basin, Turkey. *International Geology Review*, 38, 957-971.

Temiz, H., Guezou, J.-C., Poisson, A. & Tutkun, Z. 1993. Tectonostratigraphy and kinematics of the eastern end of the Sivas Basin (central eastern Turkey): Implications for the so-called 'Anatolian block'. *Geological Journal*, 28, 239-250.

van Hinsbergen, D.J.J., Maffione, M., Plunder, A., Kaymakcı, N., Ganerød, M., Hendriks, B.W.H., Corfu, F., Gürer, D.*, et al.* 2016. Tectonic evolution and paleogeography of the Kırşehir Block and the Central Anatolian Ophiolites, Turkey. *Tectonics*, 35, 983-1014.

Vergés, J., Muñoz, J. & Martínez, A. 1992. South Pyrenean fold-and-thrust belt: Role of foreland evaporitic levels in thrust geometry. *Thrust tectonics*, 255-264.

von Hagke, C., & Malz, A. (2018). Triangle zones - Geometry, kinematics, mechanics, and the need for appreciation of uncertainties. *Earth-Science Reviews,* 177, 24-42.

Weijermars, R. & Schmeling, H. 1986. Scaling of Newtonian and non-Newtonian fluid dynamics without inertia for quantitative modelling of rock flow due to gravity (including the concept of rheological similarity). *Physics of the Earth and Planetary Interiors*, 43, 316-330.

Yalçin, H. & İnan, N. 1992. Paleontologic, mineralogic and geochemical approaches to Cretaceous-Tertiary transition from Tecer Formation (Sivas). *Geological Bulletin of Turkey*, 35, 95-102.

Yalınız, K. & Göncüoglu, M.C. 1998. General geological characteristics and distribution of the Central Anatolian Ophiolites. *Yerbilimleri*, 20, 19-30.

Yalınız, M.K., Göncüoğlu, M.C. & Oezkan-Altiner, S. 2000. Formation and emplacement ages of the SSZ-type Neotethyan ophiolites in Central Anatolia, Turkey: palaeotectonic implications. *Geological Journal*, 35, 53-68.

Yetiş, C. 1968. Geology of the Çamardı (Niğde) region and the characteristics of the Ecemiş Fault Zone between Maden Boğazi and Kamışlıç. *Istanbul Üniversitesi Fen Fakultesi Mecmuası, Seri B*, 43, 41-61.

Yıldızeli, N., Akbulut, D., Ülgen, A.N., Kosal, C., Önder, O., Bulur, K., Kormalı, R., Arslan, V.*, et al.* 1984. 1/100.000 Ölçekli Açınsama Nitelikli Türkiye Jeoloji Haritaları Serisi Divrigi-G25 Paftası (l/100.000 Scaled Geological Map Series of Turkey-Divrigi G25 Sheet). *MTA Genel Müdürlügü (General Directorate of Mineral Research and Exploration, Turkey)*.

Yılmaz, A., Sumengen M., Terlemez I. & Bilgic T. 1989. 1/100.000 Ölçekli Açınsama Nitelikli Türkiye Jeoloji Haritaları Sivas-G23 Paftası.(1/100.000 scaled geological map of Turkey-Sivas G23 section). *MTA Genel Müdürlügü (General Directorate of Mineral Research and Exploration, Turkey)*.

Yılmaz, A., Uysal, Ş., Ağan, A., Göç, A.N. & Aydın, N. 1997. 1/100.000 Ölçekli Açınsama Nitelikli Türkiye Jeoloji Haritaları Sivas-F23 Paftası.(1/100.000 scaled geological map of Turkey-Sivas F23 section). *MTA Genel Müdürlügü (General Directorate of Mineral Research and Exploration, Turkey)*, 47.

Zhao, B. & Wang, X. 2016. Evidence of early passive diapirism and tectonic evolution of salt structures in the western Kuqa depression (Quele area), southern Tianshan (NW China). *Journal of Asian Earth Sciences*, 125, 138-151.

FIGURE CAPTIONS

Figure 1. Architecture of the Eastern Anatolian domain. (a) Tectonic map of the Anatolian microplate considering several crustal blocks, after Şengör & Yılmaz (1981); Robertson et al. (1991); Okay (2008); Parlak et al. (2013); Pourteau et al. (2013); Van Hinsbergen et al. (2016). (b) Geological map simplified after Bingöl (1989). (c) Synoptic cross-section across Eastern Anatolian, crosscutting the Kırşehir Block to the North, the Taurides and the south-east Anatolian orogen frontward of the Bitlis-Zagros suture zone (simplified from Legeay et al. 2018).

Figure 2. Geological Map of the Central Sivas Basin simplified from Legeay et al. (2018), built from fieldwork and previous works (Artan & Sestini, 1971; Kurtman, 1973; Yıldızeli et al., 1984; Aktimur & Tütüncü, 1988; Yılmaz et al., 1989; Aktimur et al., 1990; Poisson et al., 1996; Atabey & Aktimur, 1997; Yılmaz et al., 1997; Ribes et al., 2015; Kergaravat et al., 2016).

Figure 3. Synthetic log of the Sivas Basin associated with the mechanical stratigraphy (Legeay et al., 2018), on the basis of Ribes et al. (2015), Kergaravat et al. (2016), Kurtman,(1973), Gokten (1983), Poisson et al. (1996).

Figure 4. Synoptic cross section across the Sivas Basin, modified after Guezou et al. (1996) and Kergaravat et al. (2016).

Figure 5. Interpretation of representative seismic sections in the Sivas Basin, complemented by field observations. See Figure 2 for the location of the trace of the seismic zooms (red lines). (a) Uninterpreted and interpreted seismic section 1, illustrating the FTB and growth syncline during Eocene time. (b) Uninterpreted and interpreted seismic section 2, illustrating the STB and mother salt pinch-out that initiated backthrusting. (Seismic data courtesy from TransAtlantic petroleum Ltd.).

Figure 5 (continued). (c) Uninterpreted and interpreted seismic section 3, illustrating the triangle zone between the FTB and the STB. (d) Uninterpreted and interpreted seismic section 4, illustrating the northern Kizilrmak foreland north of the Sivas Thrust. (Seismic data courtesy from Transatlantic Petroleum Ltd.).

Figure 6. Architecture of the Central Sivas Basin. (a) Structural sketch of the Geological map, modified after Guezou et al. (1996); Kergaravat et al. (2016). The WABS domain (Wall and Bassin Structure) defined by Kergaravat et al. (2016) is encircled by red dotted line. (b) Evaporite levels in the Central Sivas Basin, showing distribution of the salt canopy and secondary generation of minibasins; modified from Kergaravat et al. (2016).

Figure 7. Uninterpreted and interpreted seismic line a-a' through the Western domain, see Figure 2 for location of the section. (Seismic data courtesy from Petroleum Transatlantic Ltd.).

Figure 8. General view of the western cross section A-A, see Figure 2 for location. (a) Regional cross section A-A' based on the interpretation of the seismic line a-a', and restored section at the top of Bozbel Formation. (b) Panoramic view of the Karacalar Anticline used to control the formations in subsurface. (c) Ophiolite thrust capped by Maastrichtian limestones (Tecer Formation) over Eocene turbidites (Bozbel Formation) belonging to the Southern edge. (d) Thrusted evaporites between a primary minibasin (Selimiye Formation) and a secondary minibasin (Karayün Formation). (e) Sedimentary wedge southward of an evaporite wall and an ophiolitic slices.

Figure 9. Uninterpreted and interpreted seismic line b-b' through the Central domain, see Figure 2 for location. (Seismic data courtesy from Petroleum Transatlantic Ltd.).

Figure 10. General view of the Central cross section B-B and associated panoramas, see Figure 2 for location. (a) Regional cross section B-B' based on the interpretation of the seismic line b-b', and restored section at the top of Bozbel Formation. (b) Contact between the ophiolite and the Taurides limestones southward of the Sivas Basin (Yilanli Mountain), with local ophiolitic mélanges at the ophiolitic sole. (c) Slices of ophiolitic basement capped by Early Eocene conglomerate (Bahçecik and Sögütlü Formations.) and Eocene evaporites (Tuzhisar Formation). (d) Emerged passive roof frontward of the Tecer Mountain over the Bozbel Formation.

Figure 11. Uninterpreted and interpreted seismic line c-c' through the Eastern domain, see Figure 2 for location. (Seismic data courtesy from Petroleum Transatlantic Ltd.).

Figure 12. General view of the Eastern cross section C-C', see Figure 2 for location. (a) Regional cross section C-C' based on the interpretation of the seismic line c-c', and restored section at the top of Bozbel Formation. (b) Çatalkaya secondary minibasin frontward of a folded primary minibasin (c) Primary minibasin (Selimiye Formation) displaying an halokinetic sedimentary wedge against a diapiric feeder (picture taken eastward of the present section).

Figure 13. Uninterpreted seismic lines and associated cross-sections perpendicular to the deformation propagation, see Figure 2 for location. (a) Cross section D-D' across the fold-and-thrust belt exhibiting the thrust stack and the passive roofing below the Selimiye minibasins. (Seismic data courtesy from Transatlantic Petroleum Ltd.).(b) Cross section E-E' across the salt-and-thrust belt domain exhibiting two minibasin generations on top of pre-salt thrust sheets.

Figure 14. Schematic tectonic evolution of the Central cross-section from the ophiolite obduction to the present-day. See text for details.

Figure 15. Examples of fold-and-thrust belts, involving synorogenic salt deposition and halokinesis as in the Sivas Basin. Cross-sections are at the same scale.

Figure 16. Comparative effects of initial salt stock in the foreland of a fold-and-thrust belt during shortening, and resulted geometry of minibasins and of the basin. See discussion for details.

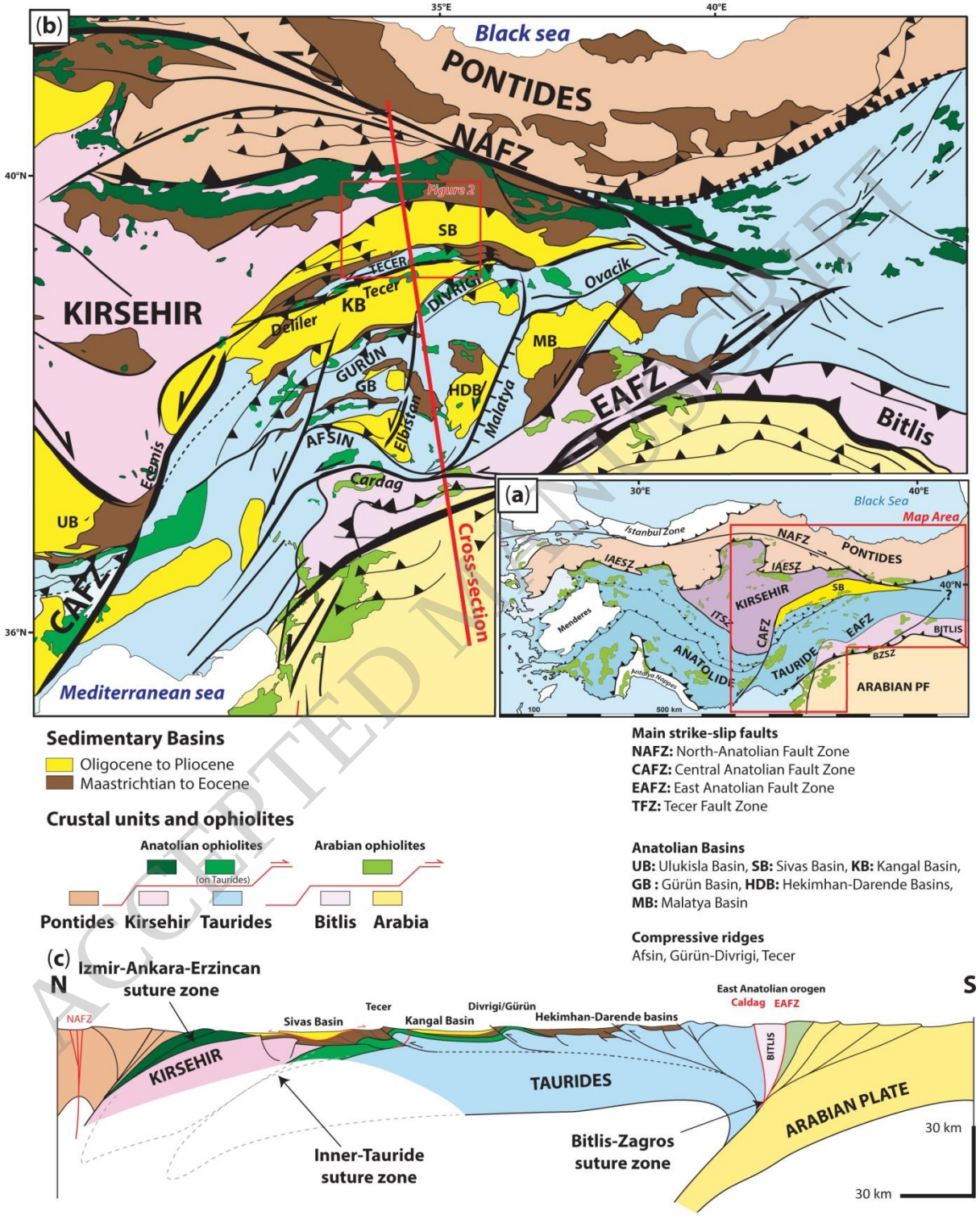

Figure 1

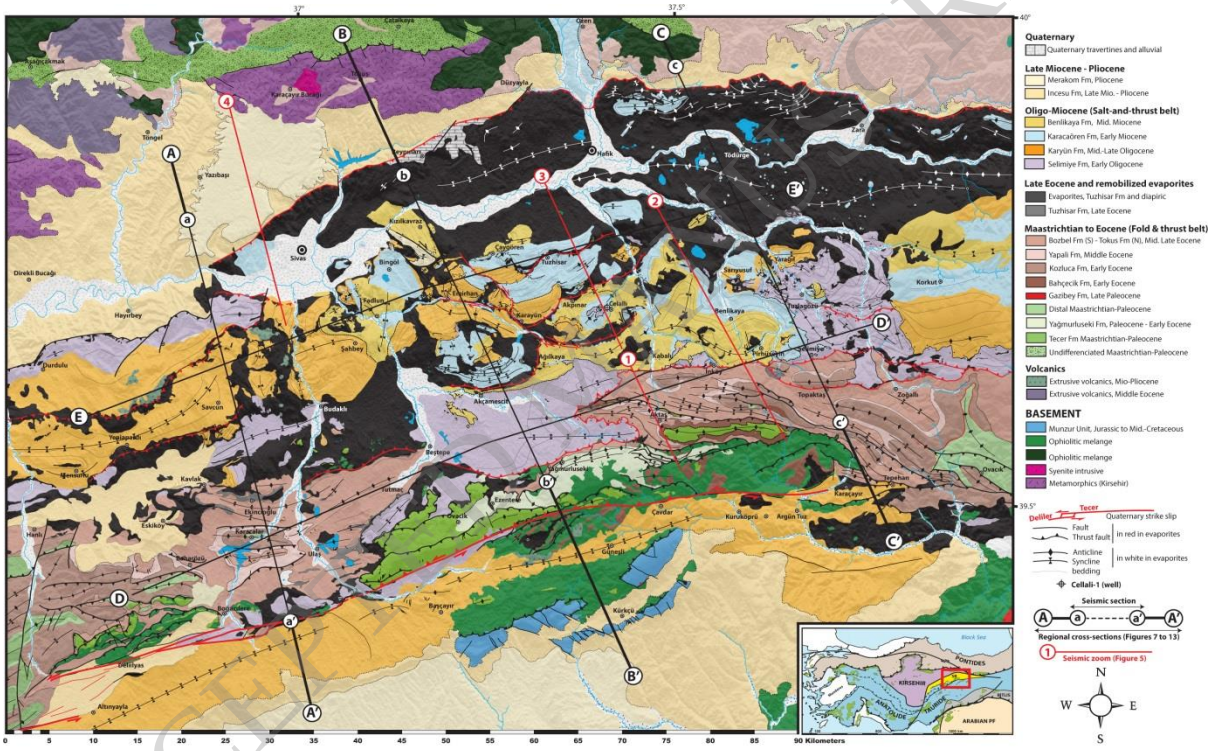

Figure 2

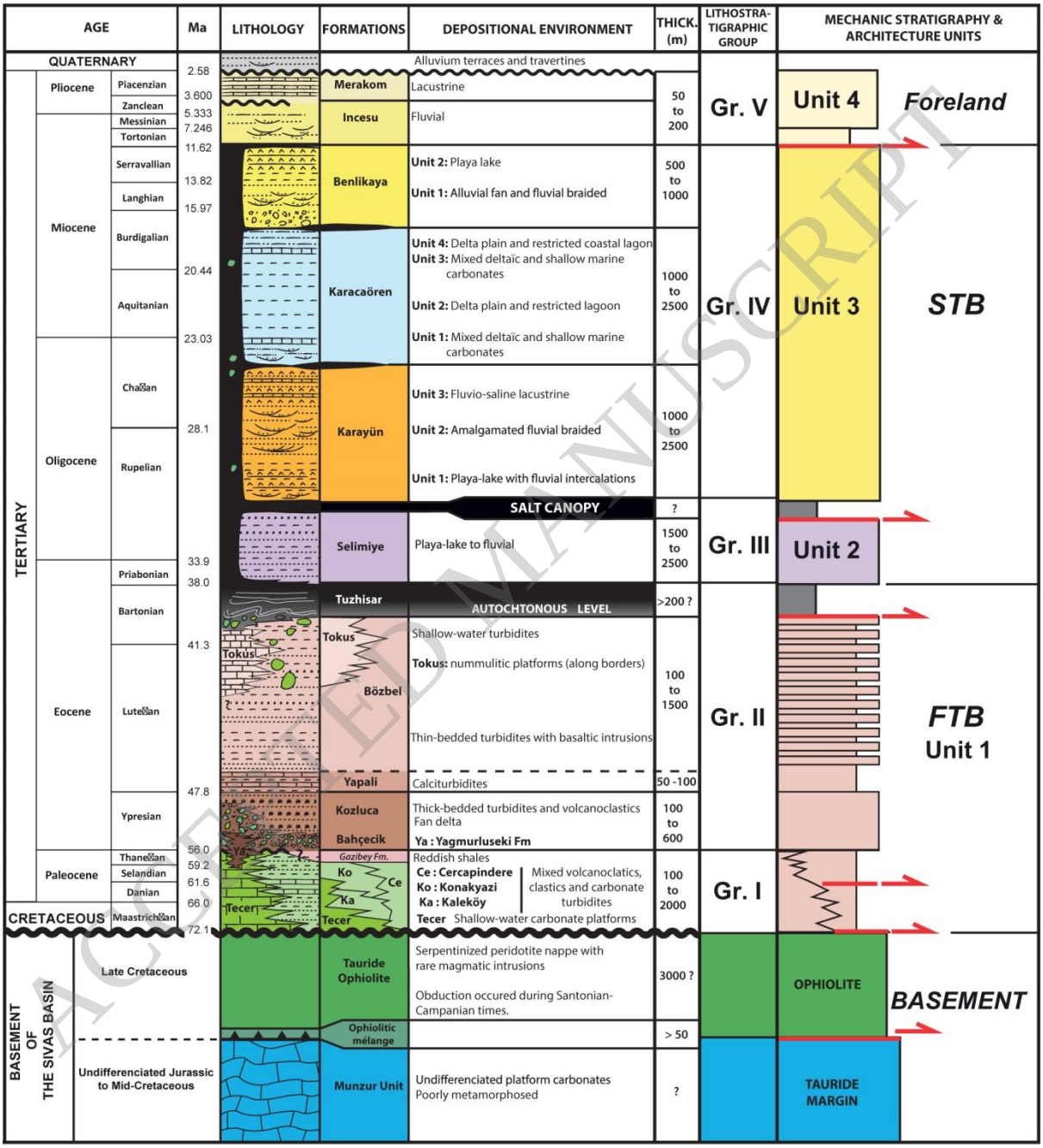

Figure 3

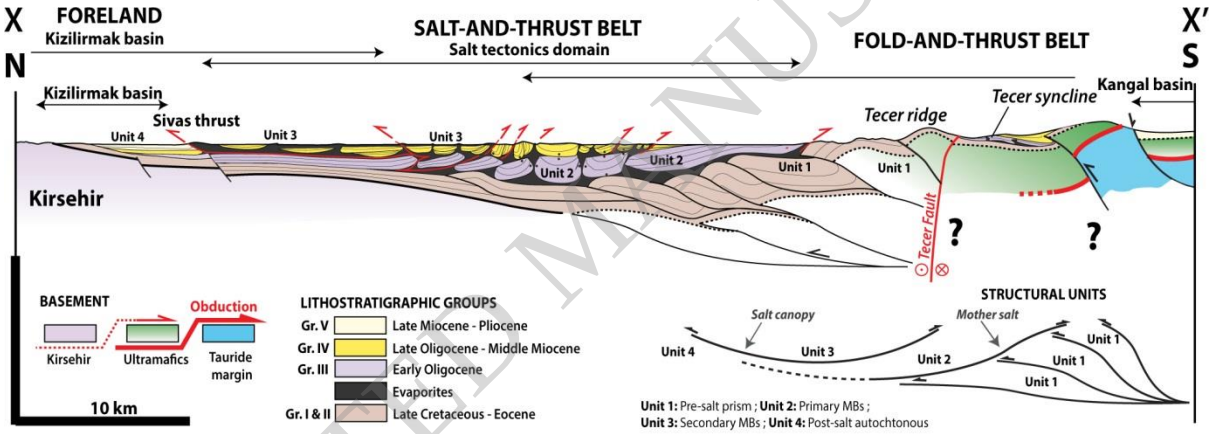

Figure 4

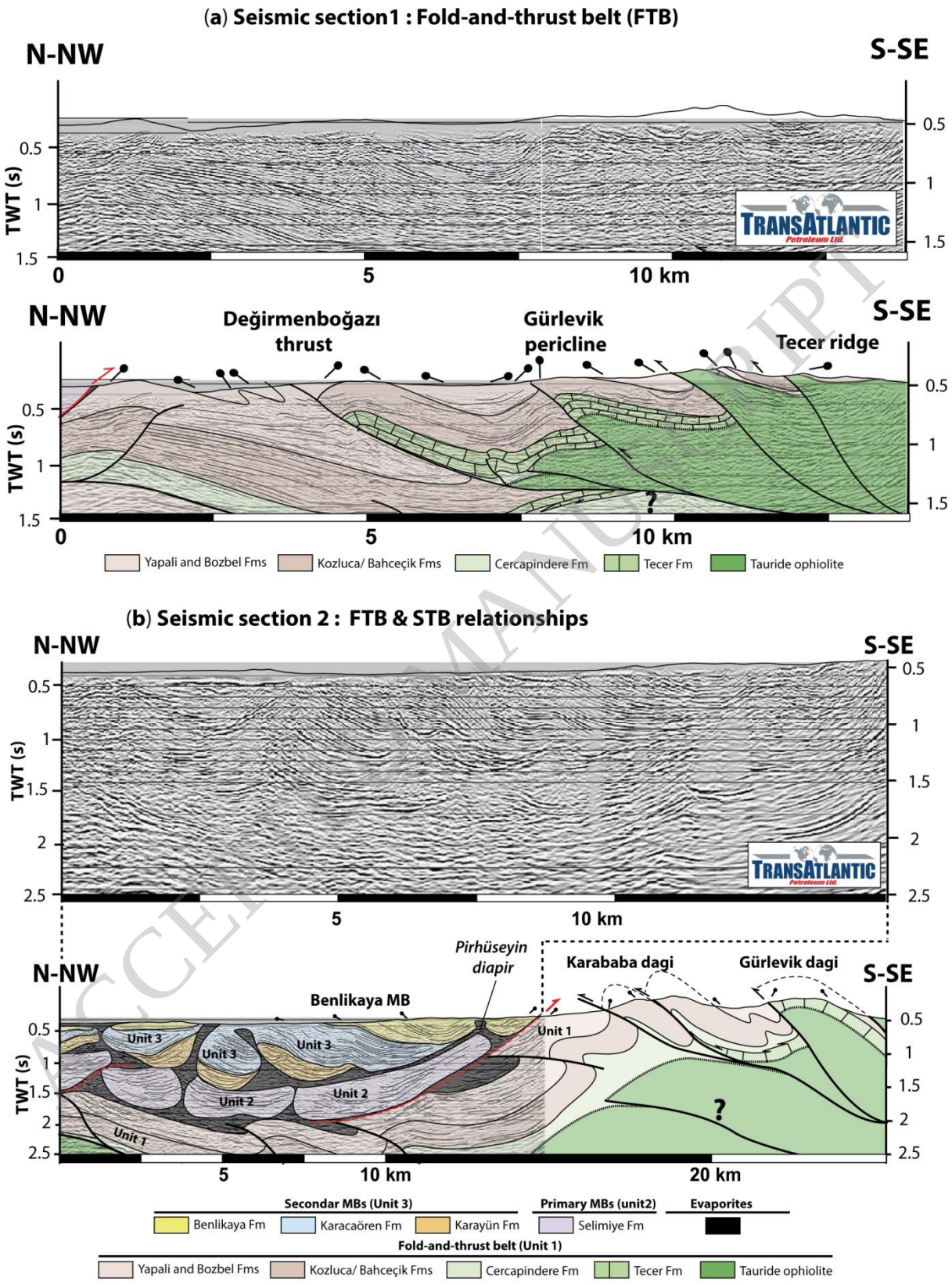

Figure 5

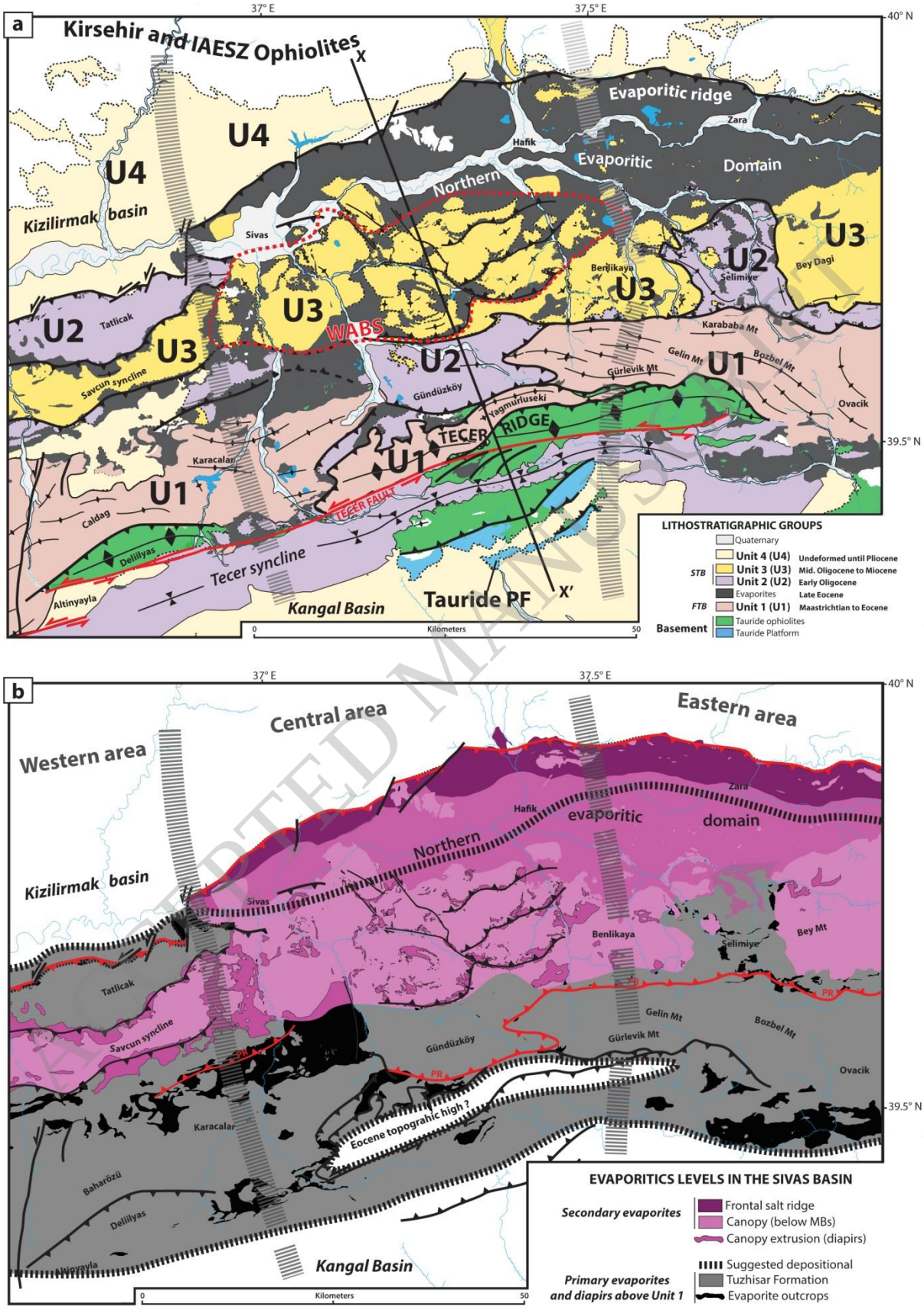

Figure 6

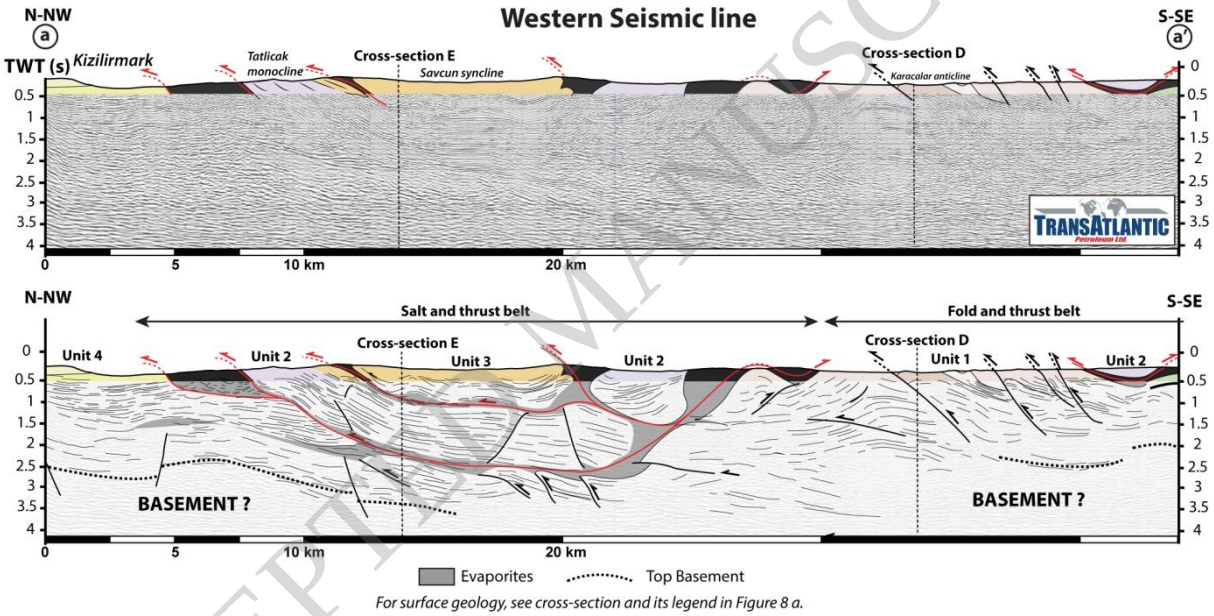

For surface geology, see cross-section and its legend in Figure 8 a.

Figure 7

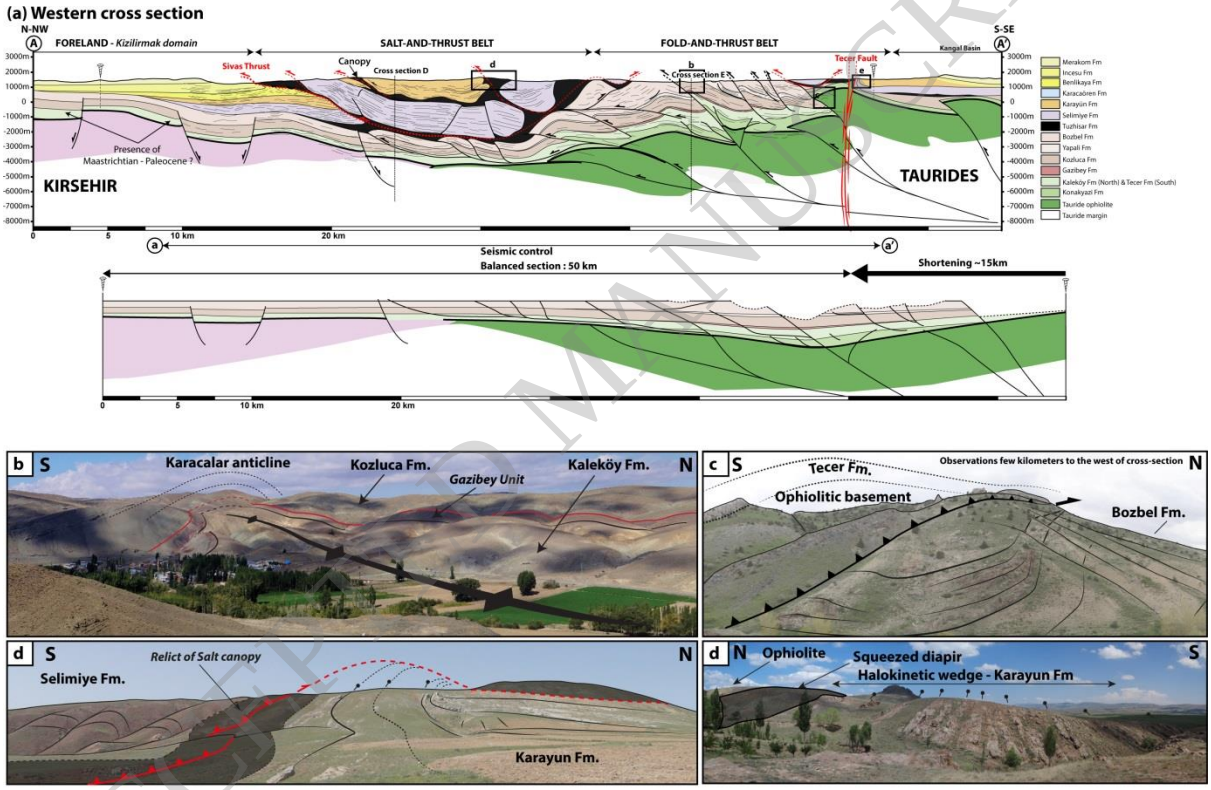

Figure 8

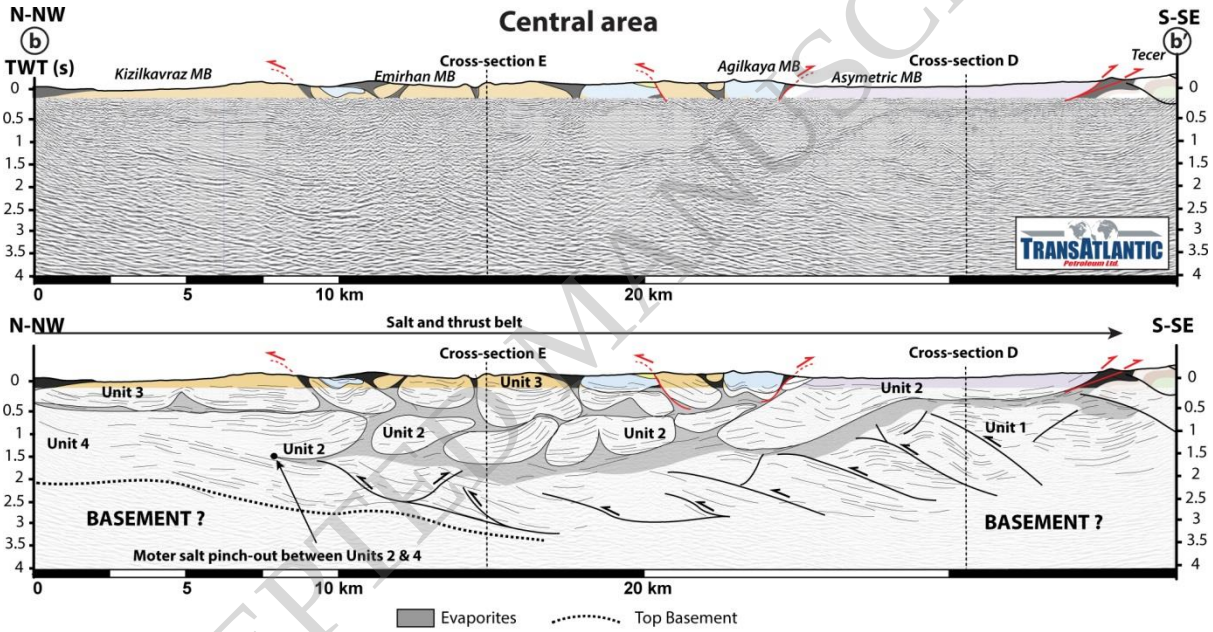

For surface geology, see cross-section and its legend in Figure 10 a.

Figure 9

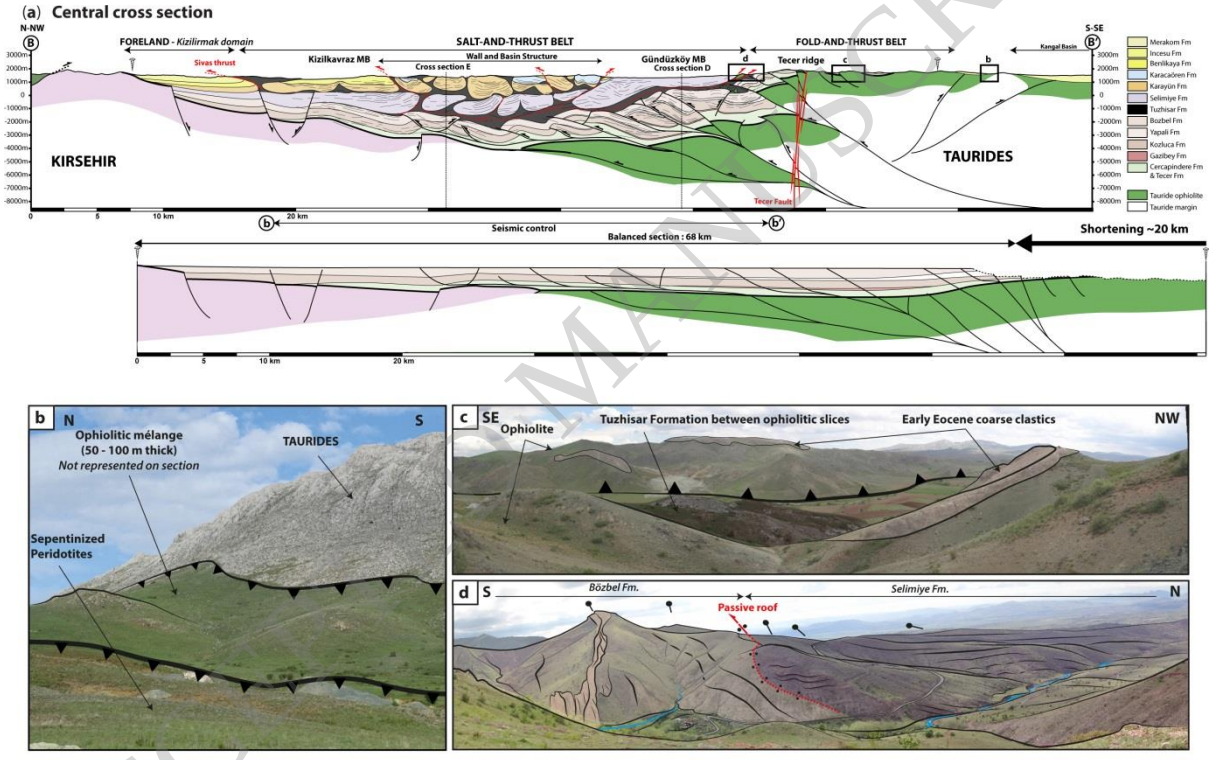

Figure 10

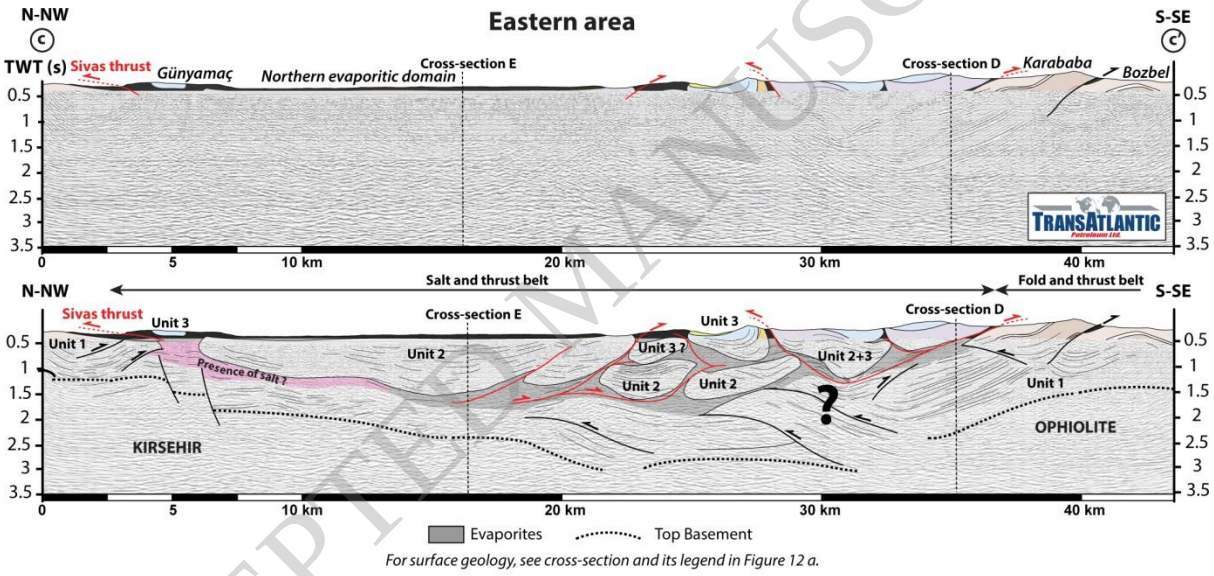

For surface geology, see cross-section and its legend in Figure 12 a.

Figure 11

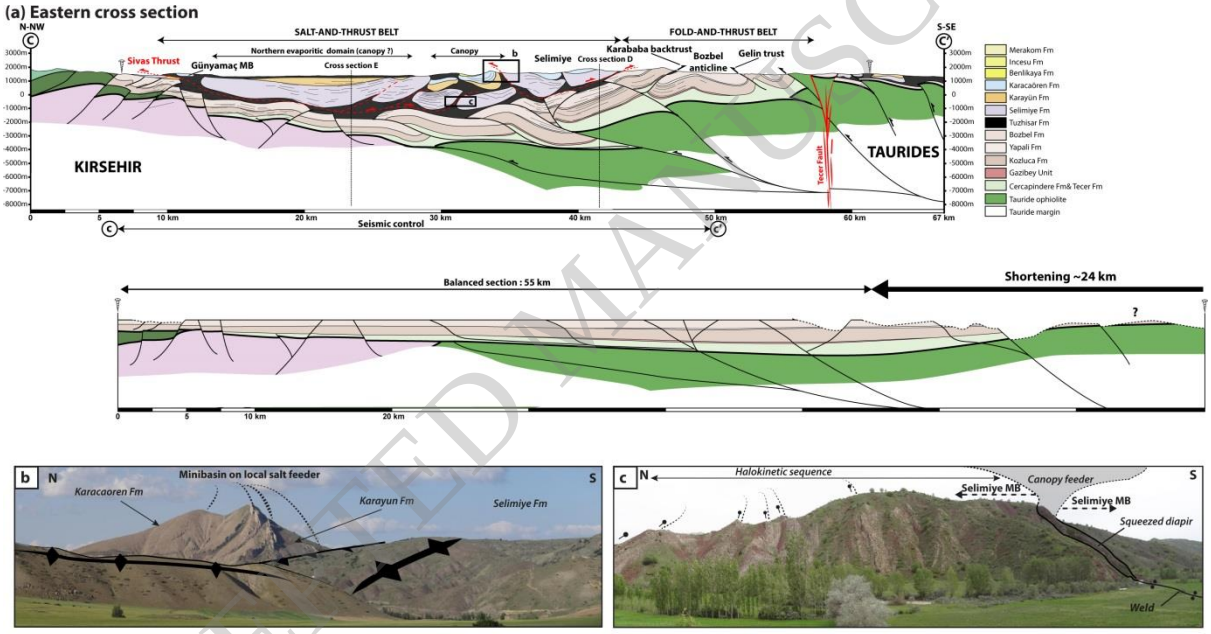

Figure 12

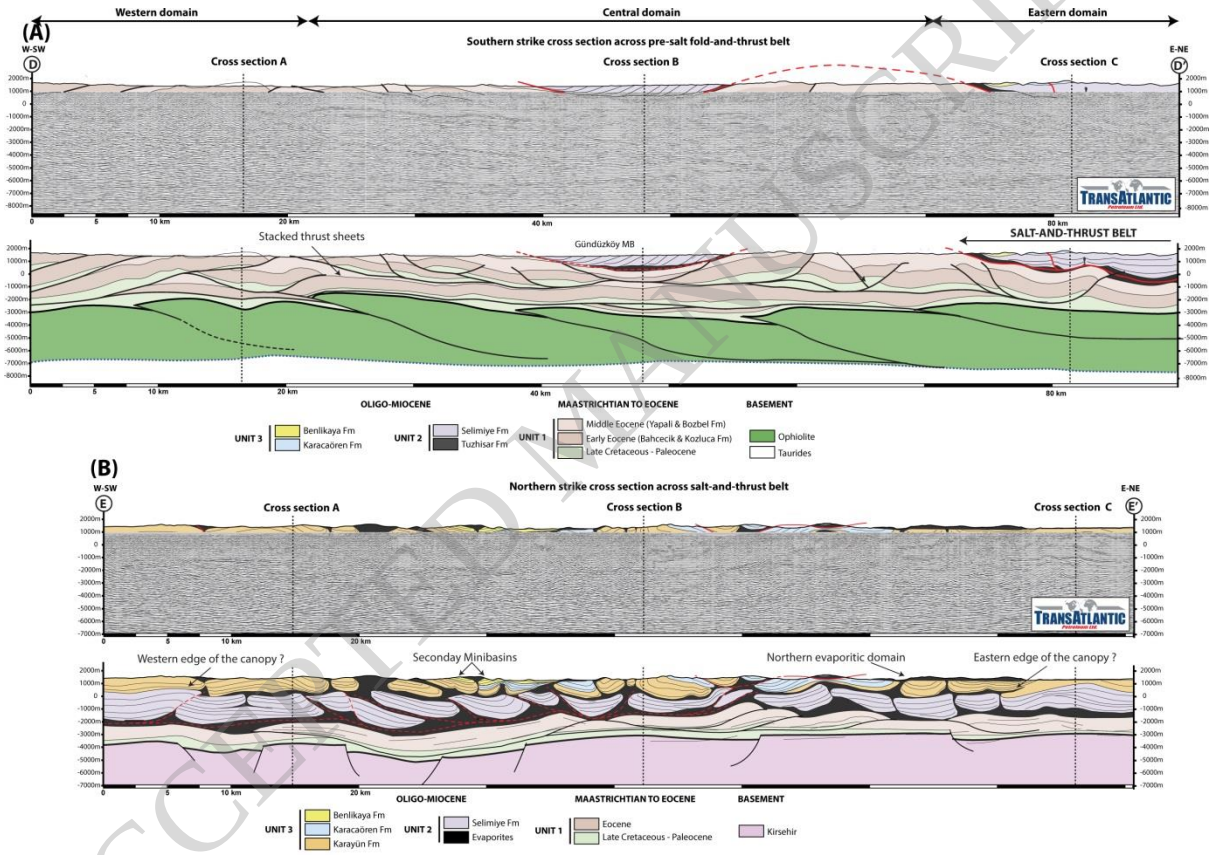

Figure 13

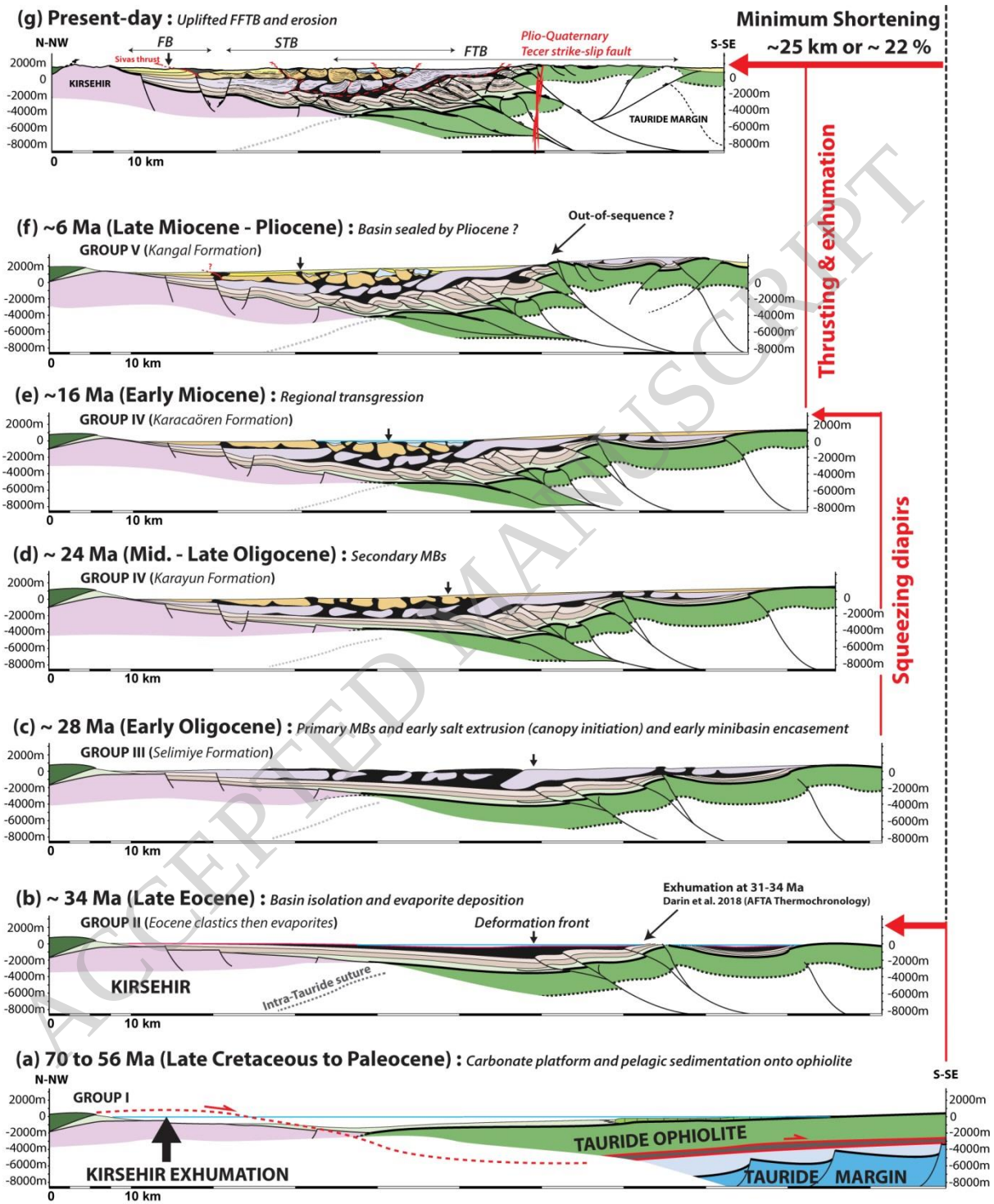

Figure 14

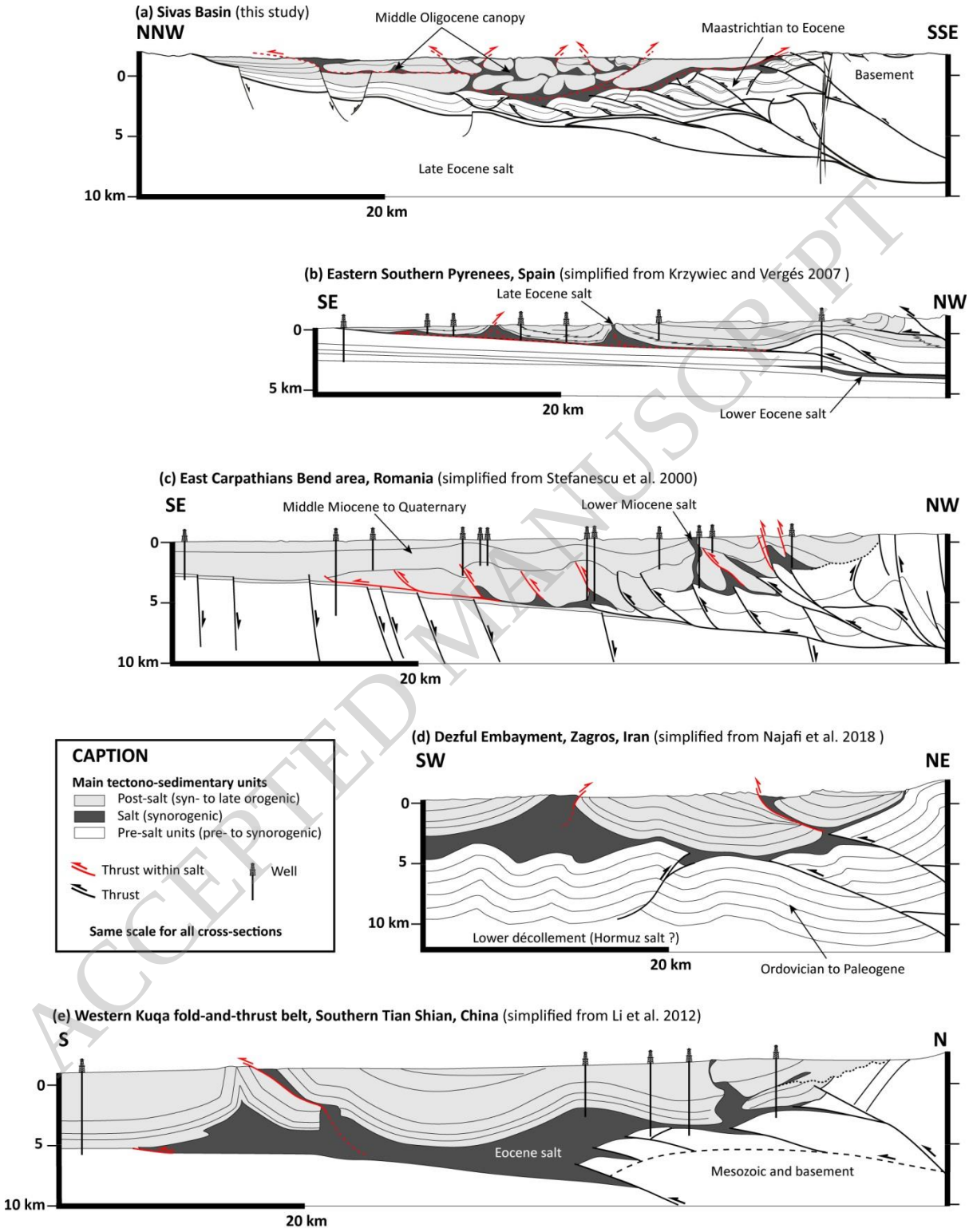

Figure 15

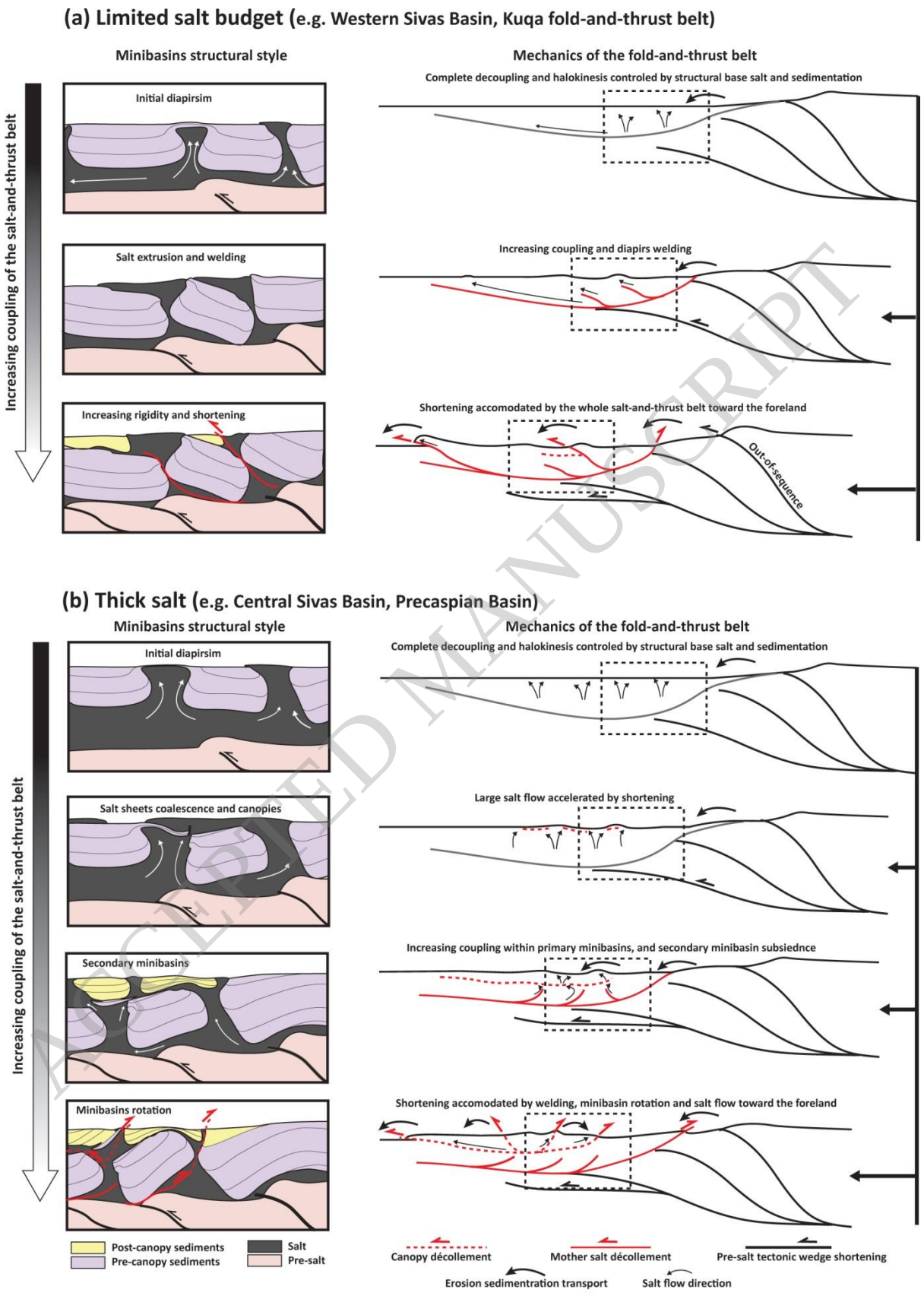

Figure 16